Physics – Uspekhi **47** (4) 371 – 391 (2004)

REVIEWS OF TOPICAL PROBLEMS PACS numbers: 61.14.Hg, 71.15.Nc, 81.05.Ea

Scanning tunneling microscopy studies of III-nitride thin film heteroepitaxial growth

R Z Bakhtizin, Q-Zh Xue, Q-K Xue, K-H Wu, T Sakurai

DOI: 10.1070/PU2004v047n04ABEH001643

Contents

Abstract. The current status of studies and new trends in obtaining and exploring surface characteristics of III-nitride semiconductors are analyzed and reviewed. Using a unique setup combining a scanning tunneling microscope (STM) with an in-line molecular-beam epitaxy (MBE) chamber, the surface atomic structures on both hexagonal and cubic GaN films grown by nitrogen-plasma-assisted MBE have been studied *in situ* over a broad range of temperatures and [N]/[Ga] ratios. Models of the observed surface phases are developed based on the comparative analysis of their atomic-resolution STM images and *ab initio* total energy calculations.

R Z Bakhtizin Department of Physical Electronics,
Bashkir State University,
450074 Ufa, Russian Federation
Tel./Fax (+7 3472) 236-574
E-mail: raouf@bsu.bashedu.ru
Q-Zh Xue, K-H Wu, T Sakurai Institute for Materials Research,
Tohoku University,
Sendai 980-7785, Japan
Tel. (+81 22) 215-2021
Fax (+81 22) 215-2020
E-mail: sakurai@imr.tohoku.ac.jp
Q-K Xue State Key Lab for Surface Science, Institute of Physics,
The Chinese Academy of Sciences,
Beijing 100080, P.R. China
Tel. (+86 10) 8264-9561
Fax (+86 10) 8264-9228
E-mail: qkxue@aphy.iphy.ac.cn

Received 14 April 2003, revised 27 October 2003
Uspekhi Fizicheskikh Nauk **174** (4) 383 – 405 (2004)
Translated by E Yankovsky; edited by A Radzig

1. Introduction

Nitrides of group III elements of the Periodic Table (from now on they will be called III-nitrides; these are three binary compounds of the Al/Ga/In-N family and their alloys, which are wide bandgap semiconductors with direct optical transitions and stable physical and chemical properties) are considered the most promising materials for developing new types of optoelectronic devices operating in the blue – green region of the spectrum, high-power rf devices capable of operating in aggressive media at high temperatures, and spintronics devices [1 – 7]. For instance, polytypes with the wurtzite structure form a continuous system of solid solutions (binary and ternary alloys) and superlattices with bandgap widths ranging from 1.9 eV for InN [1] to 3.4 eV for GaN and 6.2 eV for AlN, thus demonstrating that III-nitrides can be used to manufacture optoelectronic devices active in a wavelength range extending from red to ultraviolet.

In the 1960s, the first serious attempts were made to synthesize and study the properties of GaN, but progress in this area of research was hindered due to several formidable problems. First, there was no technology intended for bulk crystal growing, which impeded the fabrication of suitable substrates on which a high-quality material could be grown [because of the small value (0.7 Å) of the ionic radius of N, the GaN lattice parameter is much smaller than in other semiconducting III – V compounds], whereby the researchers were forced to grow the epitaxial films on substrates with a large lattice mismatch, such as sapphire [the face Al_2O_3(0001)

[1] Recently, V Yu Davydov and his colleagues from the A F Ioffe Physicotechnical Institute (St.-Petersburg) of the Russian Academy of Sciences reported that the bandgap width of InN is actually 0.7 eV (*Proc. of the 2nd All-Russia Conference on III-Nitrides*, St.-Petersburg, 3 – 4 February 2003).

was usually used]. Second, the materials fabricated by heteroepitaxial growth irrevocably demonstrated n-type conductivity, which was a result of the defect formation (usually nitrogen vacancies and impurities). The high background concentration of n-type impurities prevented p-type doping, which made formation of p – n junctions (and hence devices with such junctions) impossible [8]. An key event in this field of research was the p-type doping (by injecting an Mg impurity) achieved by Akasaki and Amano (see Ref. [9]) in 1989. Parallel to this, the development and modernization of growth techniques promoted a rise in quality of epitaxial GaN films and, in particular, a reduction in defect density, an increase in electron mobility, and, on the whole, an improvement in the characteristics of heteroepitaxial compositions.

The interest in III-nitrides grew largely because of a technological breakthrough in the development and fabrication of effective GaN-based light emitting diodes and laser diodes achieved by Nakamura et al. [10] (Nichia Chemical Industries Ltd.) in 1989. This company (Nichia) was the first to commercialize the blue and then green light emitting diodes [11], and soon after cw laser diodes operating at room temperature and emitting light with wavelengths ranging from the visible to ultraviolet (240 – 620 nm) parts of the spectrum [12]. As a result, with the three main light components (red, blue, and green) present, it became possible to design true-color LED display screens, new types of data visualization devices, traffic lights, and solid-state lighting appliances that are both durable and cost-efficient. III-nitride-based laser diodes immediately began to be used to increase the capacity of optical systems for data storage (since the packing density of the data stored in an optical medium is inversely proportional to the square of the emission wavelength), in biosensors, in high-resolution color laser printers, and in communication systems based on optical fiber lines.

Until recently, most research in the field of III-nitrides was devoted to the study of growth mechanisms, defect formation, etc., while only a few groups of researchers investigated the reconstruction of the surface of III-nitrides (one of the most important properties of such a surface). However, it is the study of the structure of a growing surface that is a problem of great importance: its solution makes possible the optimization of the conditions needed for fabricating high-quality nitride films, since the growth of subsequent layers largely depends on how the preceding layers are reconstructed. All this is highly important for improving the technology of device fabrication, since the mechanisms of nucleation and the growth peculiarities of epitaxial III-nitride films have yet to be clarified.

In many cases, the atomic structures that are formed as a result of the specific conditions of epitaxial III-nitride growth can be determined from *ab initio* calculations of the stability of surface reconstruction models. Here, the system in question must be fairly close to equilibrium state, which cannot be achieved for some superstructures that emerge in the growth process by the molecular-beam epitaxy (MBE) method [13]. Nevertheless, such a thermodynamic approximation has been successfully used to describe reconstruction and the accompanying phenomena (relaxation and the variation of the surface charge) on the surface of GaAs(001) and ZnSe(001) films grown by the MBE method, and the chemisorption Si(001) – H system by calculating the energy of surface formation as a function of the chemical potentials of the component of the compound [14]. Because of this, it is advisable to employ the same theoretical approach in representing the structure of the surface of GaN films. From the viewpoint of surface physics, the study of the reconstruction in this case is very interesting because GaN is a special case of semiconducting III – V compounds. It is synthesized from components whose atomic radii, electronegativities, and binding energies are very different, and contains both ionic and covalent bond components, so that one can expect to observe a new mechanism of surface reconstruction. At the same time, III-nitrides are polar crystals, and the polarity of the surface greatly affects the surface's atomic structure, chemical activity, and growth kinetics [15]. For GaN, the surface formation energy $E_{\rm surf}$ depends on the chemical potentials of Ga and N ($\mu_{\rm Ga}$ and $\mu_{\rm N}$, respectively) and can be written as follows:

$$E_{\rm surf} = E_{\rm tot} - n_{\rm Ga}\,\mu_{\rm Ga} - n_{\rm N}\,\mu_{\rm N}\,, \tag{1}$$

where $n_{\rm Ga}$ and $n_{\rm N}$ are the numbers of Ga and N atoms in a unit cell, and $E_{\rm tot}$ is the total energy of formation of a system consisting of Ga and N per unit cell. If the surface is in equilibrium with the bulk of GaN, then one has

$$\mu_{\rm Ga} + \mu_{\rm N} = \mu_{\rm GaN(bulk)}\,, \tag{2}$$

where $\mu_{\rm GaN(bulk)}$ is the formation energy per Ga – N pair for the wurtzite GaN crystals. Equation (2) makes it possible to exclude one of the independent variables, $\mu_{\rm Ga}$ or $\mu_{\rm N}$, and write down equation (1) for $E_{\rm surf}$ in the form of a function of the chemical potential of only one component, viz.

$$E_{\rm surf} = E_{\rm Ga} - (n_{\rm Ga} - n_{\rm N})(\mu_{\rm Ga} - \mu_{\rm Ga(bulk)})\,, \tag{3}$$

where $E_{\rm Ga}$ is the energy of system formation in the gallium enrichment mode (here, the chemical potential of GaN can be assumed to be equal to $\mu_{\rm Ga(bulk)}$). Then the difference in energies between any two reconstructions can be written as follows:

$$\Delta E_{\rm surf} = \Delta E_{\rm Ga} - (\Delta n_{\rm Ga} - \Delta n_{\rm N})(\mu_{\rm Ga} - \mu_{\rm Ga(bulk)})\,. \tag{4}$$

The chemical potential of Ga varies from the minimum value $\mu_{\rm Ga(bulk)}$ to the maximum value $\mu_{\rm Ga(bulk)} - |\Delta H_{\rm GaN}|$, where $\Delta H_{\rm GaN}$ is the heat of GaN formation, and the upper and lower limits of this range correspond to growth modes in conditions of strong enrichment, Ga/Ga-rich/ or N/N-rich/. In turn, we can assume that the thermodynamically allowed structures are those that have the lowest energy for certain values of the chemical potential of Ga from the range of admissible values [16].

To better understand the mechanisms governing the initial stages of nitride film growth, we were forced to study the superstructures on the surface of GaN films with different polarity by combining the scanning tunneling microscopy (STM), the most effective method of local diagnostics in real space with atomic resolution, and *ab initio* total energy calculations.

2. Crystal structure and polarity of III-nitrides; substrates for epitaxial growth of nitride films

In contrast to typical semiconducting III – V compounds, such as GaAs and InP, which always crystallize into the zinc blende structure, or sphalerite, films of III-nitrides crystallize

into structures of two types depending on the substrate used: a stable hexagonal structure (a lattice of the wurtzite type, the α-phase) or a metastable cubic structure (a lattice of the sphalerite type, the β-phase). Moreover, at pressures higher than 25 kbar, a structure of the rock salt (NaCl) type may form [3, 13].

The wurtzite structure has a hexagonal unit cell with two lattice parameters, a and c, whose ratio $c/a = \sqrt{8}/3 = 1.633$. The very structure consists of two close-packed hexagonal sublattices shifted by 3/8 in relation to each other along the c axis of three-fold symmetry. Both sublattices are occupied either by nitrogen atoms or by atoms of a group III element (thus, each such atom is surrounded by four nitrogen atoms). The zinc blende structure consists of two similarly oriented face-centered lattices shifted in relation to each other by one-fourth of the spatial diagonal of the cube. Just as in the wurtzite structure, each atom of the same kind is surrounded by four atoms of the other kind, and the result is a regular tetrahedron. Thanks to the tetrahedral coordination in wurtzite and zinc blende crystals, the short-range order in these two structures is almost the same, and the marked difference manifests itself only for the next three (nearest) neighbors along the direction of closest packing, which is $\langle 111 \rangle$ for the cubic structure, and $\langle 0001 \rangle$ for the hexagonal. As a result, both structures demonstrate different sequences of arrangement along the direction of close packing, and the defect in the sequence of arrangement transforms one structure into the other. Often, the two phases coexist in the defect region, which also explains why it is difficult to grow a high-purity single-phase metastable cubic III-nitride. The lattice constants and bandgap parameters of InN, GaN, and AlN crystals with wurtzite and zinc blende structures are listed in Table 1. Since neither structure has an inversion center of symmetry, the phases with cubic and hexagonal structures exhibit a sizable piezoelectric effect and crystallographic polarity: the close-packed $\{111\}$ planes in the zinc blende structure and the base $\{0001\}$ planes in the wurtzite structure differ from the respective planes $\{\bar{1}\bar{1}\bar{1}\}$ and $\{000\bar{1}\}$. In a bulk crystal, these polar planes may be limited either by cation atoms (Ga, Al, and In) or anion atoms (N). The polarity of III-nitrides is defined by the cation–anion vector along the polar axis c. If a vector $\mathbf{n}$ normal to the surface is parallel to the cation–anion vector, the films have a Ga-polarity and end in a double Ga–N layer with Ga atoms in the outer layer, and the surface is denoted (0001). In the opposite case, the films have an N-polarity (nitrogen atoms in the outer layer) and the surface is denoted $(000\bar{1})$. Notice that polarity is a bulk property, and the real surface of a film with a certain polarity can be limited either by Ga atoms or by N atoms, depending on the specific experimental conditions [3–6]. The piezoelectric coefficient in III-nitrides is almost 10 times larger than that in typical semiconducting III–V compounds [2, 4, 6].

Table 1. Lattice constants and bandgap parameters of III-nitride semiconductors [3].

Type of structure	Wurtzite			Sphalerite		
Crystal	GaN	AlN	InN	GaN	AlN	InN
Lattice constant, Å	3.18 (a) 5.18 (c)	3.11 (a) 4.98 (c)	3.53 (a) 5.96 (c)	4.52	4.3	4.9
Bandgap width, eV	3.39	6.2	1.89	3.2–3.3	5.11	22.2

The polarity of III-nitrides with the wurtzite structure is directly related to the various characteristics of the nitrides, such as the surface morphology, the height of the Schottky barrier, growth kinetics, and surface reconstruction [15]. Polarity also affects the density of defects in the epitaxial films: Ga-polar films appear smoother and have a lower defect density, which makes it possible to use them in fabricating devices [5]. Irrespective of whether the surface is polar or nonpolar (even amorphous), heteroepitaxial III-nitride films always exhibit a definite polarity. When GaN grows on a nonpolar substrate (sapphire), the growth conditions play the leading role in the polarity of the film being formed. However, when GaN grows on a polar substrate (e.g., on hexagonal SiC), the polarity of GaN films will be determined by the polarity of the substrate. Determining the resulting polarity of GaN films in relation to a given substrate constitutes an important problem, which is a part of the present work.

The high values of the binding energy (2.2 eV for GaN) are the reason for the high melting temperature of III-nitrides, a fact that seriously hinders the fabrication of crystals from melts (there is not even a phase diagram for the Ga–N system [17]). Recently, bulk crystals of gallium nitride were fabricated (TDI Inc.) via synthesis at high pressures, and they were used to grow high-quality homoepitaxial GaN films [18]. Unfortunately, such crystals are still rare and their size is limited. For this reason, the majority of III-nitrides (and even more so multilayer structures based on these nitrides) are grown by the heteroepitaxial growth technique on the substrates with mismatched lattices, and considerable effort was put into the selection of such lattices, as discussed in Refs [3, 8, 13] and in the literature cited therein. So far, GaN has been grown on Al_2O_3 (sapphire), SiC (silicon carbide), Si(111), GaAs(111), ZnO, $LiAlO_2$, $LiGaO_2$, $MgAl_2O_4$, and $ScAlMgO_4$. Among all these substrates, sapphire and silicon carbide are the most often used because of their high thermal and chemical stability, a planar morphology of the surface, and availability. GaN films of the highest quality were fabricated on just such substrates. Sapphire has several advantages over other substrates for fabricating LEDs and laser diodes, since it is transparent up to 8.8 eV and is relatively cheap. The best substrate for growing the hexagonal phase of GaN from the viewpoint of the proximity of the lattice parameters and the thermal expansion coefficients is SiC [19]. Here, SiC is also a material with great potential for fabricating high-power rf devices capable of operating in aggressive media at high temperatures, devices that cannot be fabricated from other materials.

SiC constitutes a wide bandgap material that can crystallize either into a cubic structure or into a hexagonal structure and exhibits polytypism, which is the result of different sequences of the arrangement of the double Si–C layers along the direction of closest packing. The many hexagonal and rhombohedral modifications of silicon carbide are denoted α-SiC, while the single cubic modification with the zinc blende structure is denoted β-SiC. The 6H and 4H are the most often encountered hexagonal polytypes, where the figure 6 or 4 stands for the number of layers in a single period of the sequence. The surface of SiC also possesses polarity: there is the SiC(0001) surface with protruding silicon atoms, and the SiC$(000\bar{1})$ surface with protruding carbon atoms. If the electronegativity of the elements is taken into account, one should expect the formation of a Ga-polar film (0001) on the Si-polar 6H-SiC(0001) surface, and an N-polar film $(000\bar{1})$ on the 6H-SiC$(000\bar{1})$ surface which is C-polar.

However, due to the difference in the valencies of the elements, the interphase boundary may be charged either negatively (for the Si – N compound) or positively (for the Ga – C compound). The excess charges may cause instabilities at the interphase boundary, which usually leads to fabrication of low-quality films. Film growth can be optimized by removing these charges. Unfortunately, because of its extreme hardness and chemical stability, silicon carbide is susceptible to treatment only with great difficulty and therefore the preparation of a good SiC surface (close in quality to that of GaAs or Si) proves to be a complicated problem; in particular, it is extremely difficult to remove impurity inclusions or microdefects after mechanical polishing from such a surface [20].

Metastable cubic III-nitrides were grown on substrates with cubic symmetry, such as GaAs(001), SiC(001), Si(001), and MgO (spinel) [8, 19 – 22] [2]. However, preference is given to the first two substrates even despite the fact that GaAs has a great lattice mismatch with GaN and decomposes at high temperatures. Cubic SiC (3*C*-SiC) has a lattice constant that is much closer to that of β-GaN and, in addition, remains stable at high temperatures, which is preferable for growing high-quality epitaxial films with cubic symmetry. Here, one of the problems associated with the fabrication of cubic SiC is that the crystals proper are grown by the heteroepitaxial growth technique on an Si(001) substrate which has a large lattice mismatch with SiC (Hoya Corp.).

In addition to the difficulties encountered in matching the parameters of the epitaxial layer and the substrate, a serious problem is presented by the large difference in the binding energies of gallium and nitrogen atoms (the binding energy of nitrogen atoms is 1.5 times higher than that of common semiconducting III – V compounds [24]). GaN films with good structural and electrical characteristics are fabricated via chloride – hydride vapor-phase epitaxy (HVPE), metalorganic chemical vapor deposition (MOCVD), and MBE [3, 21, 25].

Because of the high deposition rate, the HVPE method is applicable when thick III-nitride films and low-temperature buffer layers need to be fabricated. The MOCVD method combined with the lateral buildup technique makes it possible to fabricate GaN films of the highest quality with a minimum number of defects ($\leqslant 10^8$ cm^{-2}), a low electron concentration ($\sim 10^{16}$ cm^{-3}), and a planar morphology of the surface [12, 26], so that at present most devices based on III-nitrides are fabricated by the MOCVD method. At the same time, the MBE method makes it possible to control the thickness of the growing layer with high accuracy (up to monatomic) at relatively low temperatures and in supersaturation conditions, with the quality of the fabricated films sometimes comparable to that achieved by the MOCVD method. The highly nonequilibrium situation in conditions of MBE growth can be used to grow multilayer structures in which individual layers retain their chemical integrity and compositionally form distinct interphase boundaries with each other. This feature makes the MBE method capable of fabricating structures with superlattices based on III-nitrides, with the relatively low growth temperature being a favorable condition for growing In-containing III-nitride alloys (the presence of In in the active layer is the reason for the formation of deep localized states in which electron motion is restricted in all three dimensions). III-nitrides can be grown by the MBE method if one uses plasma-activated nitrogen impurities, which facilitates their introduction into the near-surface layer. At the same time, MBE is an ultrahigh-vacuum technique compatible with a broad spectrum of surface analysis/diagnostics methods, such as reflection high-energy electron diffraction (RHEED), ellipsometry, Auger-electron spectroscopy (AES), and STM.

[2] Kurobe et al. [23] have reported on growing the cubic GaN on sapphire which has hexagonal symmetry.

3. Experimental technique

3.1 A combined installation: the MBE – STM chamber

The major experiments were carried out with a unique combined installation that included an ultrahigh-vacuum scanning tunneling microscope (with a base pressure of $\sim 3 \times 10^{-11}$ Torr maintained in the measuring chamber) arranged in-line with a molecular-beam epitaxy chamber (ULVAC Ltd.), with the two forming a single vacuum system (see the review article [27]). This installation made it possible to perform *in situ* studies of the surface structure and morphology of epitaxial films. The MBE chamber contained six Knudsen cells, each with one shutter controlled independently from the other shutters, and a reflection high-energy electron diffractometer (Fig. 1). The flux of Ga atoms from a Knudsen cell was stabilized in such a way so as to maintain a relative concentration [N]/[Ga] that would ensure a two-dimensional growth of films. To introduce nitrogen atoms into a growing GaN layer, they must be activated, since at room temperature N_2 molecules are fairly inert and do not react with group III elements because of the strong triple bonds between two nitrogen atoms. To dissociate N_2 molecules or nitrogenated molecules into neutral atoms or ions that are active even at room temperature [3, 13], researchers use plasma sources based on electron cyclotron

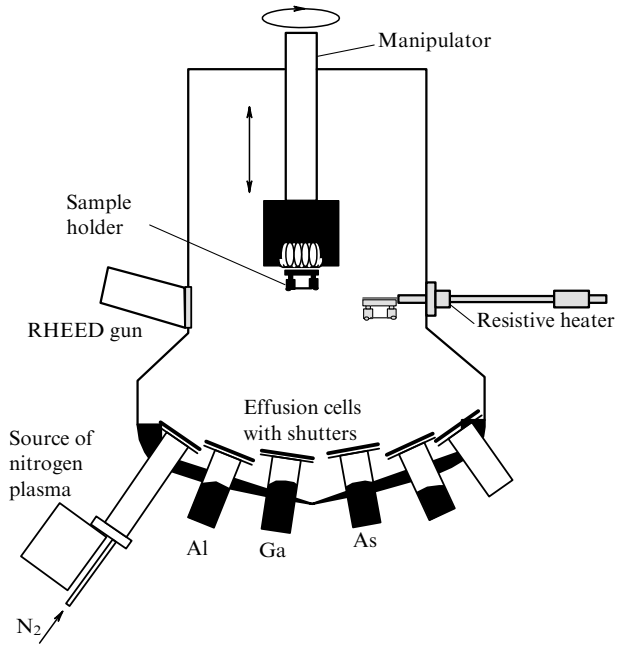

Figure 1. MBE installation for growing III-nitride films. (Since SiC is transparent, there was no way in which the substrate temperature could be raised above 700 °C by using the standard heater built into the MBE chamber, so the samples were heated resistively with the help of a specially designed sample holder.)

resonance (ECR) or an rf discharge. ECR sources ensure bigger fluxes of active nitrogen components and make it possible to achieve higher film growth rates. Their drawback, however, is that they produce a large number of high-energy ions which substantially damage the epitaxial layer, so that the quality of nitride films is reduced. The rf plasma sources produce low-energy ($\leqslant$ 10 eV) singly charged molecular ions or neutral nitrogen atoms [13], thus substantially reducing the risk of radiation damage and making it possible to grow high-quality III-nitride films. We used an rf source with an output power of 250 W (EPI Corp.).

For scanning probes we used tungsten tips manufactured by electrolytically etching single-crystal tungsten wire with the $\langle 111 \rangle$ orientation (FEI Corp.), and graded tips manufactured from a Pt–Ir alloy (Unisoku Ltd.). To estimate the usefulness of the probing tips and the possibility of modifying their shape and cleaning the surfaces from possible contamination in the course of the experiments, the scanning tunneling microscope was equipped with a built-in field ion microscope.

3.2 Preparing a clean 6*H*-SiC(0001) surface

During epitaxial growth, the atomic structure and morphology of the substrate surface directly affect the structure of the growing crystal and defect formation, so that preparing a clean surface plays a crucial part in the successful fabrication of heteroepitaxial III-nitride films. The lattice constant and the thermal expansion coefficient of 6*H*-SiC are most close to those of GaN, but preparing a clean surface of 6*H*-SiC (in particular, the removal of impurity inclusions or microdefects after mechanical polishing) proved to be extremely difficult [20], which has for a long time prevented the use of such a substrate. For instance, high-temperature warm-up in an ultrahigh vacuum does not remove oxides and impurities from the surface; rather, it results in silicon depletion of the near-surface layer and leads to graphitization of the surface [28]. Kaplan [29] proposed removing oxides from the SiC surface by treating it with Si or Ga beams, since this promotes the formation of a volatile compound SiO or Ga_2O. The potential of this approach was also demonstrated by STM method [30]. Another way to remove thick oxide layers is to etch the surface with HF [31]. Neither way removes mechanical damage (scratches, etc.), however. On the other hand, etching in hydrogen is not selective and produces mirror-smooth surfaces, while the reaction products comprise gaseous hydrocarbons and the initial silicon [32], with the result that it can be used to prepare the SiC surface. However, STM studies have shown that additional treatment is needed here [33].

To clean the SiC surface, we developed a two-step method which includes high-temperature treatment in an atomic hydrogen atmosphere and *in situ* etching in an Si flux in an ultrahigh vacuum [34]. Using this approach, we were able to prepare an atomically clean 6*H*-SiC(0001) surface, grow epitaxial GaN films on it, and study the atomic structures of these films [35]. According to the procedure we developed, a sample of the 6*H*-SiC(0001) surface was first cleaned in an ultrasonic bath filled with acetone/methanol, then etched in a stream of atomic hydrogen (20%) and argon (30%) in a specially designed furnace at 1600 °C, and finally placed in the chamber for preparing samples, where it was degassed at 650 °C for a long time in an ultrahigh vacuum. The same chamber was used to etch the sample in an Si flux with an intensity of $10^{14}-10^{15}$ cm^{-2} s^{-1}. The etching procedure consisted of covering the sample's surface with several layers of Si at 850 °C and warming up by a series of flashes up to 1000 °C in an Si flux. Usually, 10 cycles of this kind were sufficient for cleaning the surface.

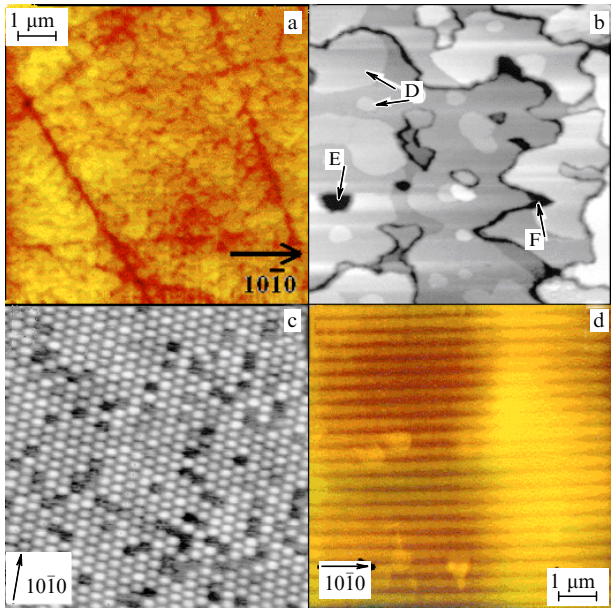

Figure 2. (a) AFM image of the starting 6*H*-SiC(0001) substrate. (b) STM image of this surface after etching in an Si flux (scanned area was 2500×2500 Å^2, bias voltage between sample and probing tip was $V_s = -3.0$ V, and tunnel current $I_t = 4.0 \times 10^{-11}$ A). (c) Enlarged image of a distinct part of the same surface (195×280 Å^2). (d) AFM image of the 6*H*-SiC(0001) substrate after etching in hydrogen.

Figure 2a shows the image of the surface of a large area of the starting 6*H*-SiC(0001) plate, obtained by an atomic-force microscope (AFM) in air. Because of the presence of a natural oxide on the surface, no topographical features are observed and no stepped structure manifests itself. Mechanical scratches formed in the process of polishing the sample are displayed as dark streaks distributed at random over the surface. The root-mean-square value of the height of the inhomogeneities is about 60 Å.

Etching in an Si *flux*. This leads to desorption of silicon oxide because of the formation of volatile monoxide and makes it possible to avoid carbonization/graphitization due to silicon depletion of the near-surface region at higher annealing temperatures [29]. In the STM image of the occupied states of a surface subjected to such treatment (Fig. 2b) one can clearly see two-dimensional SiC islets (denoted by arrows with a D), dimples (denoted by an arrow with an E), and grooves in the form of dark twisted lines (denoted by an arrow with an F) that have formed as a result of mechanical polishing. Note that in the areas corresponding to macroscopic scratches (dark strips in Fig. 2a), scanning became unstable. This suggests that such areas were not affected by the Si beam. A high-resolution STM image (Fig. 2c) shows that, despite the formation of locally ordered regions with a 3×3 reconstruction, the surface treated in an Si flux consists largely of terraces of irregular shapes separated by randomly oriented steps of varying height. One could expect that etching at higher temperatures (> 1100 °C) would speed up the decomposition of SiC [28] and would therefore facilitate the removal of scratches, but no significant changes in the surface morphology were discovered.

Etching by hydrogen atoms in combination with etching in an Si *flux*. After the surface undergoes high-temperature etching in hydrogen, the situation changes dramatically. The AFM image (Fig. 2d) clearly demonstrates the advantages of hydrogen etching: now the surface is composed of evenly distributed terraces (light stripes) separated by straight steps (dark streaks in the image), which extend for at least 10 μm along the $\langle 10\bar{1}0\rangle$ direction. The terrace width in the vertical direction is 0.4 μm, and the root-mean-square value of the difference in heights of the inhomogeneities does not exceed 15 Å (which is four times smaller than the previous value), which clearly indicates an improvement in the surface morphology. However, STM studies of this surface have shown that its structure is also disordered, and annealing in an ultrahigh vacuum only at times led to formation of locally ordered domains with a $\sqrt{3}\times\sqrt{3}$ structure [33], thus proving the need for further treatment.

Figure 3 shows STM images of the occupied states of the sample surface after etching in hydrogen and treatment in an Si flux. Clearly, the treated surface consists of clean flat (at the atomic level) terraces separated by straight steps oriented along the $\langle 10\bar{1}0\rangle$ direction (see Fig. 3a), with the surface free of both macro- and microscratches (they are taken off). Note that the high-resolution images may exhibit, depending on the conditions in which the surface was prepared, a 3×3 reconstruction (Fig. 3b) which did not change when a small amount of aluminium was introduced (Fig. 3c). Clearly, Al forms a two-dimensional islet. Annealing at 700 °C was found to lead to desorption of the entire amount of Al, which suggests that aluminium has a low reactivity with respect to silicon. Changing the Si concentration in the flux, one can also arrive at a $\sqrt{3}\times\sqrt{3}$ reconstruction (Fig. 3d), which agrees with the results of other researchers (see Refs [29, 30, 36]). The height of all the steps is about 15 Å and equals six times the height of a unit step of the 6*H* polytype. The uniform height distribution of the steps indicates that the outer layer of all the terraces ends with a double Si – C layer belonging to the very sequence of arrangements that has the lowest surface energy [37], while the equal distance between adjoining steps may be the result of their mutual repulsion [38]. The structure and morphology of the observed atomically clean SiC surface (see Fig. 3) are comparable in quality to the thoroughly studied Si and GaAs surfaces, which proves the effectiveness of the two-step method of sample cleaning. The mean value of the width of the evenly arranged terraces, determined from STM images, equals 4100 ± 20 Å, i.e., the very value we observed in an atomic-force microscope (Fig. 2a), while the sample's disorientation angle lies within 0.5°, which agrees well with the specifications provided by the company that manufactured the sample (Cree Res. Corp.).

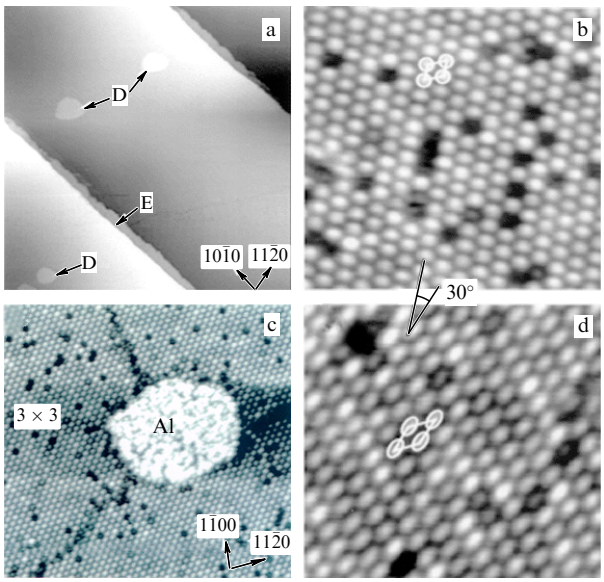

Figure 3. STM images of an atomically clean 6*H*-SiC(0001) surface ($V_s = -3.0$ V, and $I_t = 8.0\times 10^{-11}$ A). (a) Scanned area 5000×5000 Å^2 [here, D is a two-dimensional islet whose height is equal to that of the double layer of SiC ($2H = 2.5$ Å), and *E* is a 4*H* half-step near a normal 6*H* step]. (b) High-resolution image showing a 3×3 reconstruction (scanned area 84×95 Å^2). (c) Image of the same surface after deposition of a 0.05 Al single layer at room temperature and subsequent annealing at 600 °C for 10 min (scanned area 180×200 Å^2). (d) High-resolution image showing a $\sqrt{3}\times\sqrt{3}$ reconstruction (scanned area 124×95 Å^2).

After slight modifications, this method was also used to clean the C-polar 6*H*-SiC surface.

3.3 Preparing a clean 6*H*-SiC(000$\bar{1}$) surface

As noted earlier, the acute problems in preparing a clean SiC surface are the removal of scratches and other damage caused by polishing, as well as of oxides and contaminants remaining on the surface. Bernhardt et al. [39] applied the procedure of hydrogen etching to the 6*H*-SiC(000$\bar{1}$) surface, i.e., to the C-polar surface of 6*H*-SiC, and obtained an ordered surface morphology, which was demonstrated by LEED method. Note, however, that hydrogen etching was done at temperatures so high that the inhomogeneity of heating could lead to cracking of the surface, with the result that in some cases in the removal of oxides the researchers were forced to use only etching in an Si flux to avoid graphitization and retain the stoichiometry of the surface.

Before the 6*H*-SiC(000$\bar{1}$) samples were placed in the vacuum chamber, they were flushed in an ultrasonic bath containing acetone/methanol. The AFM image of the surface of the starting sample (Fig. 4a) shows that the surface is very coarse and contains randomly oriented scratches and grooves that appear as a result of mechanical polishing, while a stepped structure does not manifest itself. After degassing at 650 °C in an ultrahigh vacuum and carrying out ten etching cycles in an Si flux, the surface became flat and its image demonstrated the presence of broad terraces, up to 0.4 μm wide, separated by twisted steps (Fig. 4b). Here, the surface exhibited neither microgrooves nor dimples, which indicates that all mechanical damage was removed by etching in the Si flux. Analysis of STM images made it possible to identify two types of steps (indicated by arrows): A (of height $4H = 10$ Å), and B (of height $2H = 5$ Å), which produce two types of terraces belonging to different packing sequences in the 6*H*-SiC structure. Estimates of the size distribution of these terraces have shown that the overall area of the terraces with A-steps exceeds that of the terraces with B-steps, and therefore the former has a lower surface free energy and higher stability than the latter. What is important is that in the case of Si-polarity of the 6*H*-SiC substrate, etching in the Si flux alone was not enough to remove all mechanical damage. Such difference in behavior may be related to the higher rate of decomposition of the C-polar surface of 6*H*-SiC. In addition, the structure of randomly oriented steps on the 6*H*-SiC(000$\bar{1}$) surface (Fig. 4b) differs significantly from the structure of the 6*H*-SiC(0001) surface prepared by hydrogen etching (see Fig. 3a), where all steps are strictly straight and

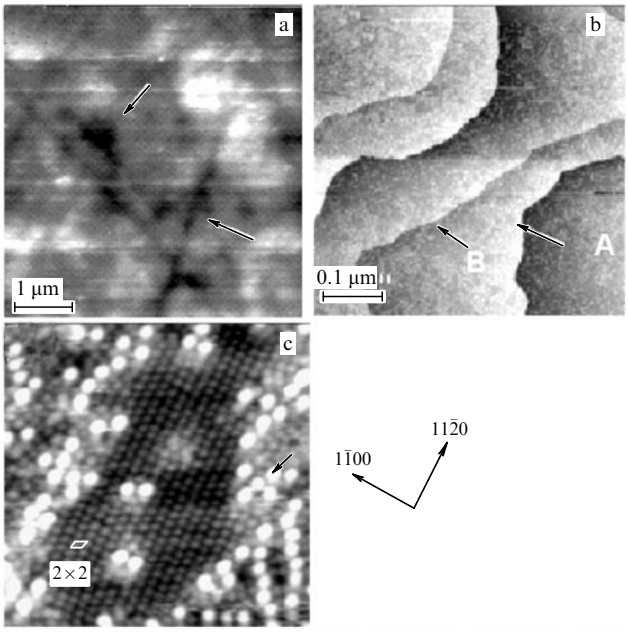

Figure 4. (a) AFM image of the starting $6H$-SiC(000$\bar{1}$) substrate (scanned area is 5×5 μm ^{2}; the arrows point to scratches and microdimples that formed as a result of mechanical polishing). The difference in the heights of the light and dark areas amounts to 20 nm. (b) STM image of occupied states of the same surface after etching in an Si flux (the arrows at A and B point to steps with the heights $4H$ and $2H$, respectively). (c) STM image of the $6H$-SiC(000$\bar{1}$) surface with a 2×2 structure ($V_s = -2.6$ V, $I_t = 1.0 \times 10^{-10}$ A, and scanned area is 100×100 Å^2).

have the same height equal to six times the height of the Si – C double layer ($6H = 15$ Å).

Several reconstructions were observed on the C-polar surface of $6H$-SiC. By warming up the samples in an ultrahigh vacuum without etching in Si, Bernhardt et al. [41] observed 3×3 and 2×2 structures [41], while warming up the samples in an Si flux led to formation of an Si-enriched 2×2 reconstruction. Other researchers also reported on observations of Si-enriched $\sqrt{3} \times \sqrt{3}$, 2×2, 3×3, and $2\sqrt{3} \times 2\sqrt{3}$ reconstructions in the same conditions [30, 39, 43]. In our studies, after warming up the sample in an Si flux at 1050 °C, we observed a 2×2 LEED pattern in which some of the $2\times$ reflections were absent. Figure 4c presents the image of this surface with atomic resolution, which shows that the 2×2 phase is not quite ordered: in addition to the 2×2 structure there are randomly distributed bright spots that demonstrate a tendency to form chains along the close packing direction $\langle 11\bar{2}0 \rangle$. To establish the nature of these spots, we deposited Si on the surface under study at room temperature and then heated the surface to 900 – 950 °C. For high coverage of the surface this led to formation of an Si(111)-7×7 structure, while in the case of submonolayer coverage the region with the 2×2 reconstruction became disordered but the bright spots remained visible. Heating to higher temperatures in order to remove the Si-coverage led to restoration of the 2×2 structure, but the distribution of bright spots did not change, and so it was concluded that these spots are caused by the tunneling from the C atoms that remained after evaporation of the silicon atoms, which agrees with the results of Bernhardt et al. [39, 41] and Starke et al. [42].

4. Surface atomic structures of wurtzite GaN films, grown on Si-polar and C-polar $6H$-SiC substrates

Hexagonal epitaxial GaN films grown along the polar axis of the substrate always exhibit a definite polarity, namely, either a Ga-polar (0001) surface or an N-polar (000$\bar{1}$) surface is formed, which agrees with the electronegativity of Ga and N and preferable formation of Si – N and C – Ga bonds at the interphase boundary [15, 44, 45]. At the same time, analysis of the results of recent STM studies and *ab initio* calculations [46 – 48] made it possible to establish new aspects in the mechanism of minimization of the surface energy, aspects that are connected with the surface polarity and cannot manifest themselves in ordinary III – V compounds but may affect surface reconstruction.

Generally speaking, the emergence of superstructures in the surface of GaN may proceed in the traditional way through the formation of new bonds between surface atoms during their relaxation or between atoms of the surface and the adsorbate. Because of structural relaxation accompanied by charge transfer or effects of strong electron correlation between the highest occupied and the lowest unoccupied surface states (HOMO and LUMO), a gap forms that finally produces a semiconducting or insulating surface furthering the lowering of the surface energy. However, structural relaxation distorts the bonds of the surface atoms in the local surroundings, thus generating a surface stress field that is added to the surface energy. The final surface atomic structure is determined by the balance between the gain in energy caused by the reduction of the number of dangling bonds and the expenditure of energy caused by the surface stress formed. In the case of the surfaces of polar semiconductor compounds, the reconstruction mechanism gets more complicated because of the possible changes in the surface stoichiometry, and the electron counting rule becomes then useful in checking the stability of the superstructures formed [49 – 51].

4.1 Thin GaN(0001) films grown on a $6H$-SiC(0001) substrate

The first studies of superstructures on the GaN(0001) surface were done by the RHEED method. The phases 1×1, 2×1, 2×2, 2×3, 2×4, 3×2, 3×3, 4×4, 4×6, and 5×5 were observed, but the results contained no detailed information about the atomic structure, and no correlation between the phases and the film polarity was found [51 – 57]. Later on, *ab initio* total energy calculations were done for the 2×2 reconstruction and models of possible stable atomic structures were proposed [58 – 61], which were not verified in experiments, however. The first systematic STM and RHEED studies of the surface structures on GaN films with a known polarity were carried out by a group headed by R M Feenstra (see Refs [46, 47, 62 – 64]). For an N-polar surface grown on sapphire by the MBE technique, the researchers observed 3×3, 6×6, and c(6×12) reconstructions, while for the homoepitaxial film with a Ga-polar surface they observed the 2×2, 5×5, and 6×4 phases, so that the significant effect of polarity on the surface structure was corroborated via direct comparison of the structures of the films grown on different substrates.

In our experiments we began growing GaN films by first nitridizing an atomically clean $6H$-SiC(0001)-3×3 surface. Then at 750 °C we deposited a 150-Å thick buffer AlN layer,

which made it possible to reduce lattice mismatch (the mismatch between the GaN and AlN lattices amounted to 2.6%, while that between the AlN and SiC lattices amounted to 1%). Finally, the substrate temperature was lowered to 650 °C, and the GaN films were grown in gallium-enrichment conditions with a rate of roughly 1000 Å h^{-1}. Note that the growth of films in nitrogen-enrichment conditions was accompanied by the observation of a discontinuous RHEED pattern, while the growth of films in gallium-enrichment conditions produced a RHEED pattern in the form of distinct strips. All growth was stopped by quenching the nitrogen plasma. The procedure was followed by deposition of two Ga monolayers at the growth temperature and rapid cooling of the sample. As a result of film growth over the course of two hours, the surface acquired a characteristic interference coloring and a 1×1 RHEED pattern was observed. If a single Ga monolayer was deposited on such a surface at room temperature and then the sample was annealed at 200 °C in the course of roughly 10 min, a 2×2 phase appeared. This phase corresponds to a stable growth front for which the fabricated GaN films are of the highest quality. It is taken as the base for the (0001) surface. Further annealing at 250 °C led to the appearance of the surface 4×4 and 5×5 phases. The 4×4 structure could also be produced by depositing more than one Ga monolayer on the 1×1 surface and annealing the sample at 250 °C for 10 min. The $5\sqrt{3} \times 2\sqrt{13}$, $\sqrt{7} \times \sqrt{7}$, and 10×10 reconstructions and the pseudo 1×1-Ga fluid phase could be produced in the same way by depositing one or two Ga monolayers on the surface with a 1×1 structure as the coverage thickens, and subsequent annealing at 200 – 400 °C.

For a detailed study of the surface structure it was crucial to determine the polarity of the film. To GaN films grown on an Si-polar 6*H*-SiC substrate, we assign Ga-polarity. Here are the reasons for doing so:

(1) After Ga or Al was deposited (from a submonolayer to three monolayers) on a 6*H*-SiC(000$\bar{1}$) substrate and the sample was annealed at a low temperature ($\leqslant$ 600 °C), no noticeable changes in surface morphology or new structure creation were detected, except for the formation of several two-dimensional or three-dimensional Al islets or Ga droplets randomly distributed over the surface (the number of droplets or islets depending on the thickness of the deposited layer). Annealing at higher temperatures (up to 700 °C) led to the desorption of all Al/Ga islets. One example of this is shown in Fig. 3c, where the deposited aluminium forms a two-dimensional islet, while the surrounding 3×3 structure remains undamaged, which suggests that the reactivity of Al with respect to Si is low and that the chemical bond N – Si is predominant at the interphase boundary [65].

(2) In their research, Feenstra's group repeatedly observed 1×1, 3×3, 6×6, and c(6×12) structures on the films of (000$\bar{1}$) polarity [46] and 2×2, 5×5, and 6×4 reconstructions in the films of (0001) polarity [47]; the polarity of the GaN/SiC system proper was set via chemical etching. Similar results were obtained by other groups of researchers (e.g., see Ref. [15]). In our experiments, conducted under similar conditions, we observed a series of superstructures involving 2×2, $\sqrt{7} \times \sqrt{7}$, 4×4, 5×5, $5\sqrt{3} \times 2\sqrt{13}$, and 10×10, which agrees with the results obtained for the (0001) surface.

To control the polarity of the III-nitride surface, attempts were made to begin the growing of films with the nitridation of a C-polar substrate or the deposition of Al/Ga on an Si-polar substrate. However, no good films were produced along this avenue of research, which could be due to the mixing of the Ga – Si and N – Si bonds, which in the long run leads to poor crystallization. According to the recommendations made in Refs [15, 47, 51], to control polarity, GaN films were subjected to chemical etching, but the morphology changed very little after this, which suggested that the surface was inert to chemical action, in agreement with the assumption of Ga-polarity. Hence, we suggest that the GaN films grown on 6*H*-SiC(0001) substrates are Ga-polar, namely, GaN(0001) films, while those grown on 6*H*-SiC(000$\bar{1}$) substrates are Si-polar.

4.2 Surface reconstructions on the Ga-polar GaN(0001) face

The GaN-1×1 *surface*. Figure 5a illustrates a typical morphology of the GaN surface that formed immediately after the growing stopped. The surface has a distinct terrace – step structure, with the height of the steps amounting to 2.55 Å and equal to the height of a double layer of hexagonal GaN along the polar axis *c*, while the size of the smooth sections reaches 0.5 μm, which unquestionably proves the advantages of an SiC substrate and the need to use an AlN buffer layer. In accordance with the preparation conditions and the observed 1×1 RHEED pattern, such a (rapidly cooled) surface corresponds to the bulk 1×1-Ga structure. However, despite the plain morphology, the enlarged image of the same surface (Fig. 5b) exhibits no ordered structure. One can see many dark holes roughly 10 Å in diameter (indicated by arrows) that are randomly distributed over the surface, which suggests that the formation of a complete Ga monolayer was not finished.

The 2×2 *and* 4×4 *phases*. Figure 5c shows a typical STM image of the occupied states of the structural 2×2 phase characterized by regularly arranged rows of bright dots separated by a distance of 6.4 Å along both directions of close packing. Figure 5d depicts the image of the 4×4 phase formed because of the absence of every second row of bright dots in the 2×2 structure. The 4×4 phase was prepared by annealing the 2×2 phase, which presupposes partial desorption of Ga from the surface, with the result that the 4×4 phase is less enriched with Ga than the 2×2 phase. Figures 5e – g present the various models of the 2×2 structure, predicted theoretically in Refs [59 – 61]. Depending on what model one chooses, the rows of bright dots in Fig. 5a can be considered the result of tunneling from dangling bonds of N, Ga adatoms of the outer layer or other occupied surface states. The N-adatom model (Fig. 5f) can be excluded immediately, because it is improbable that the surface was enriched in N in such conditions of surface preparation, but the Ga-adatom model (Fig. 5e) corresponds to these conditions. This model satisfies the autocompensation rule [49 – 51], so that the 1×1-Ga atoms occupying sections with threefold symmetry (indicated by the arrow in Fig. 4c) should not be considered atoms of the first surface layer (rest atoms) [66], and their dangling bonds remain unoccupied. For the same reason, one should not expect a significant contribution from the 1×1-Ga atoms to the STM images of occupied states, and we associate the bright dots in Fig. 4a with the tunneling from Ga atoms of the outer layer.

According to Fritsch et al. [59], a structure with a Ga adatom proves to be stable only within a limited range of values of the Ga chemical potential, and in conditions of lower Ga content the Ga-vacancy model is preferable (Fig. 5g); hence, it would be interesting to establish how this

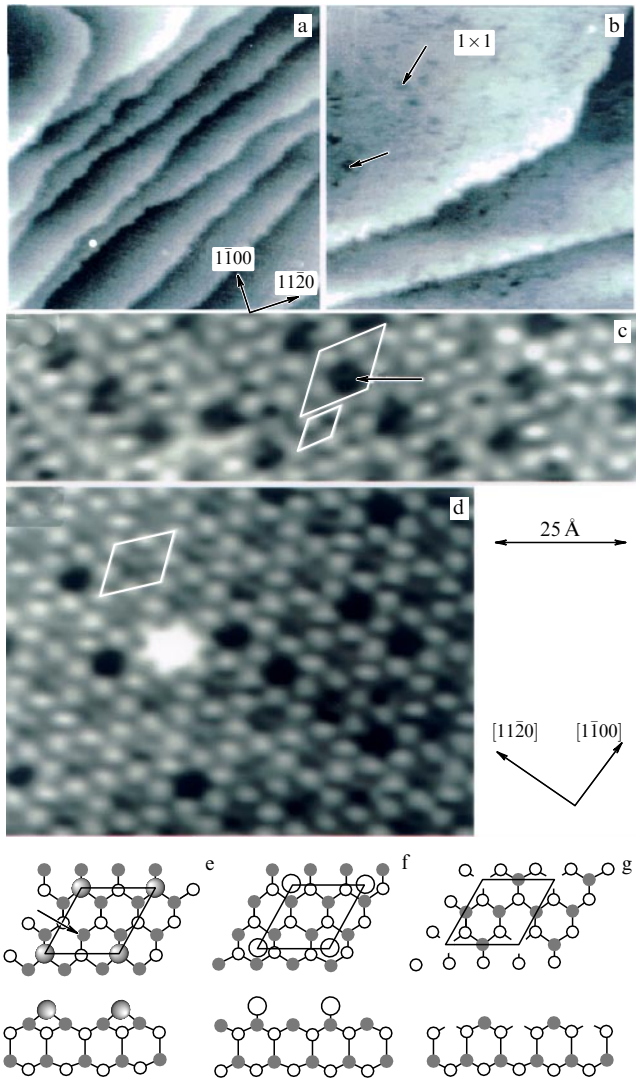

Figure 5. STM images of the occupied states of the GaN(0001) surface: (a) immediately after termination of the growth process, scanned area is 1500 Å × 1500 Å; (b) enlarged image of the same surface (250 × 200 Å^2); (c) image of the 2 × 2 phase, and (d) image of the 4 × 4 phase ($V_s = -2.8$ V and $I_t = 8.0 \times 10^{-11}$ A). Geometrical models (top and side views) of the GaN(0001)-2 × 2 structure: (e) the Ga-adatom model (the Ga adatom, the large hatched circle, occupies the area T_4 directly above a nitrogen atom belonging to the second layer; it is assumed that the gap between the adsorbed layer and the 1 × 1-Ga layer amounts to 1.73 Å); (f) the N-adatom model (the N adatom, the large light circle, occupies the area H_3, and a Ga atom that is bonded to an N atom proves to be elevated by 0.15 Å), and (g) the Ga-vacancy model (dark and light circles of a smaller diameter represent Ga atoms of the first layer and N atoms of the second layer).

model agrees with the STM image of the 2 × 2 phase (Fig. 5a). In this structure, three-fourths of an electron from each dangling Ga bond transfers to three dangling bonds of the N atom of the second layer. In our vacancy model, which is discussed below, the remaining Ga atoms of the 1 × 1 structure relax downwards by 0.39 Å, while N atoms of the second layer move up by 0.01 Å. In this case, the occupied surface states formed by N atoms become accessible for analysis by STM and must dominate in tunneling in the occupied state mode. Thus, it is impossible to select a correct model by basing one's reasoning only on the analysis of STM images.

Solving this problem required doing *ab initio* total energy calculations for all the models within the framework of the density functional formalism. The highly localized nature of the 2s and 2p electrons of nitrogen and 4d electrons of gallium hindered *ab initio* calculations, and therefore we used the Troullier – Martins 'soft' pseudopotentials [65, 68] (the results are given in Fig. 6). The calculated value of the heat of GaN formation proved to be $\Delta H_{\mathrm{GaN}} = 1.4$ eV, which agrees with the experimental value of 1.14 eV, and the relative stability of the different structures was defined as a function of the Ga chemical potential within the range of thermodynamically allowed values:

$$\mu_{\mathrm{GaN(bulk)}} - \Delta H_{\mathrm{GaN}} \leqslant \mu_{\mathrm{Ga}} \leqslant \mu_{\mathrm{GaN(bulk)}} \,.$$

Figure 6a demonstrates that the most stable structures are those that are described by the Ga-adatom and N-adatom

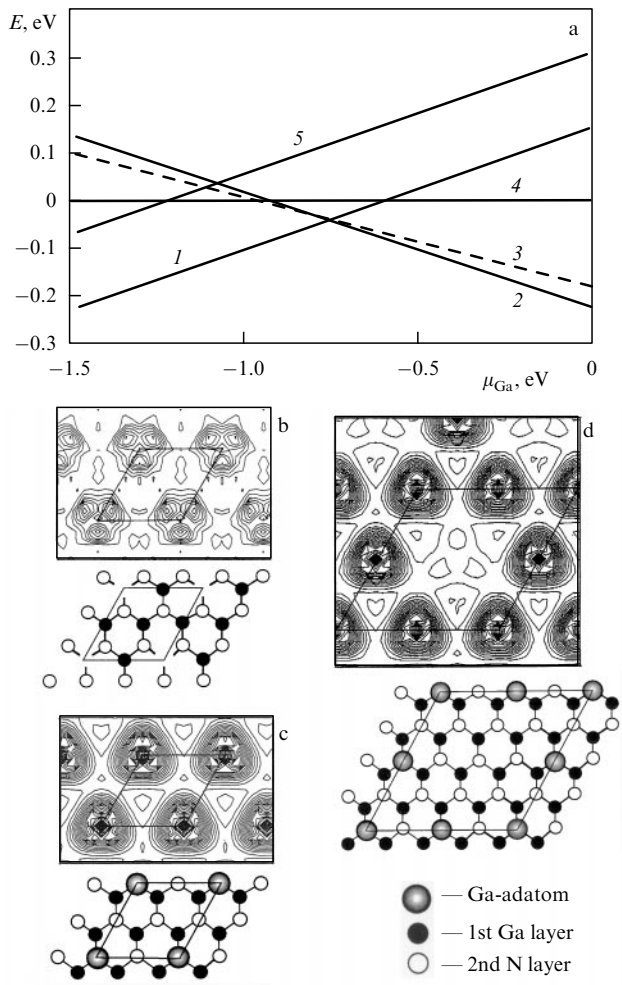

Figure 6. (a) The surface formation energy as a function of the Ga chemical potential, calculated for the GaN(0001) face with respect to the bulk GaN-1 × 1 structure: for the N-adatom model, the 2 × 2 reconstruction (line *1*); for the Ga-adatom model, the 2 × 2 reconstruction (*2*); for the absent Ga-adatom model, the 4 × 4 reconstruction (*3*); for the 1 × 1-Ga structure (*4*), and for the Ga-vacancy model, the 2 × 2 reconstruction (*5*). The surface charge density distributions calculated for the GaN(0001) face: (b) the 2 × 2 reconstruction, the Ga-vacancy model; (c) the 2 × 2 reconstruction, the Ga-adatom model, and (d) the 4 × 4 reconstruction, the absent Ga-adatom model. The local density of states was calculated by integrating the contributions from the states of the valence band that are located 2 eV below the HOMO band at a level of 1.3 Å above the outer surface layer.

models in conditions of gallium and nitrogen enrichment, respectively (the straight lines *1* and *2*). In calculating the charge density we assumed that it is the sum of contributions from the states in the valence band that encompass a region 2 eV below the highest occupied molecular orbital (HOMO), which agrees with the conditions in which STM studies are conducted ($V_s \leqslant -3.0$ V). Notice the good agreement of the observed STM images with the results of calculations done according to the Ga-adatom model (Fig. 6c), although, despite the expected formation of pairs of 2p-orbitals of N atoms located in the sections with three-fold symmetry of the basal plane (0001), the charge distribution calculated by application of the Ga-vacancy model proved to be split in space (Fig. 6b) and did not agree with the results of the experiment.

Note that Ramachandran et al. [69] related the emergence of a 2×2 structure on the Ga-polar GaN(0001) surface to the presence of arsenic impurity used in growing GaAs films (a small amount of this impurity could have remained in the MBE chamber). As shown by the same group of researchers (see Ref. [70]), a similar effect may be produced by the adsorption of Mg in the process of growing GaN films. Later, the effect of arsenic impurity on the formation of the 2×2 reconstruction was corroborated by Vézian et al. [71], but here the 4×4 structure was observed only if an additional amount of Ga had been deposited on the surface 2×2 phase (i.e., for a thicker layer of Ga). The researchers related this fact to the use of ammonia (instead of nitrogen plasma) for nitridizing the surface and a more precise estimate of the amount of Ga.

Let us return to the 4×4 phase (see Fig. 5). The STM images depict several 4×4 cells (indicated by white lozenges) that have formed because of the absence of several bright dots (indicated by arrows). Note that in the course of annealing at 200 °C to 300 °C the 2×2 and 4×4 phases usually coexist. The transition to the 4×4 phase, which occurs as the temperature rises and is accompanied by a loss of some of the Ga atoms/adatoms, made it possible to assume that the 4×4 phase is formed because of the Ga desorption from the 2×2 surface. The model of an absent adatom (Fig. 6d) was developed to explain the 4×4 reconstruction, and it agrees fairly well with the experimental results. A theoretical analysis of this model, made by using equations (3) and (4), has shown that within a broad range of allowed values of the Ga chemical potential ($-0.72 \leqslant \mu_{Ga} \leqslant 0$ eV) the model of the 4×4 phase (straight line *3* in Fig. 6a) is preferable energetically to all other structures, with the exception of the Ga-adatom model of the 2×2 structure (straight line *2* in Fig. 6a). According to this model, the Ga content in the 2×2 and 4×4 phases is 1.25 and 1.18 monolayer, respectively. When the Ga content is lower than these values, both models become comparable in energy, and since the 4×4 and 2×2 phases are very close in structure, we can assume that the activation energy needed for the corresponding phase transition is low. Earlier, we noted that in the phase transition from the 2×2 structure to the 4×4 structure in each unit cell one bright dot with a periodicity of $2\times$ (the factor of $\times$ indicates the number of lattice periods) is lost, appearing in the image as a dark spot (Fig. 5d). In the model of the 4×4 phase (Fig. 6d), the vacancies in the outer layer of Ga adatoms are arranged within a triangular lattice, and the electrostatic repulsion between the charged Ga adatoms stabilizes such a configuration.

The 5×5 *phase and quasi-one-dimensional chains of* Ga *atoms*. The conditions required for the preparation of a 5×5 phase differ little from those that have been used in the case of 4×4 phase, and so far no real difference in their formation has been established. This fact has made it possible to assume that their surface stoichiometries are almost the same. Studies of the 5×5 structures revealed that the RHEED patterns have distinct, but discontinuous, lines along the $\langle 11\bar{2}0 \rangle$ direction, and when the electron beam impinged on the sample along the $\langle 1\bar{1}00 \rangle$ axis, strong background noise emerged. A typical STM image of the 5×5 phase, where the latter phase coexists with the 4×4 phase (Fig. 7a), exhibits a specific feature of this structure, namely, uniformly arranged linear chains aligned with the $\langle 11\bar{2}0 \rangle$ direction. The distance between these chains, measured along the $\langle 1\bar{1}00 \rangle$ direction, proved to be 15.8 Å, which is roughly $5a_0$ [$a_0 = 3.19$ Å is the lattice constant of the GaN(0001) face)]. A high-resolution image (Fig. 7b) shows that each chain is actually formed by a sequence of pairs of dots (i.e., each line is a doublet). The distance between the points depends on the periodicity of the arrangement and is 6.4 Å ($2\times$), 9.6 Å ($3\times$) or ~ 7 Å ($2.5\times$), and there are more points separated by ~ 7 Å (almost 50%), which as a result leads to one-dimensional disorder along the $\langle 11\bar{2}0 \rangle$ direction.

Thus, the 5×5 structure is even devoid of a unit cell, in contrast to the 2×2 and 4×4 phases, and does not belong to the family of $N \times N$ superstructures [60]. Therefore, it is advisable to describe it as a 5×2.5 superstructure [65]. If the observed dots correspond to tunneling from Ga adatoms, some of these adatoms may occupy positions between the lattice sites, which suggests that atomic relaxation has occurred.

According to the results of measurements of the scanning profiles (Fig. 7a), the contrast of the 5×5 phase exceeds that of the 4×4 phase only by 0.15 Å, which is irrevocable proof that this is a poor electronic effect. Basing our reasoning on the absent Ga-adatom model of the 4×4 structure (Fig. 6d), the conditions required for preparing the 5×5 phase, and the analysis of STM images, we developed a geometrical model of

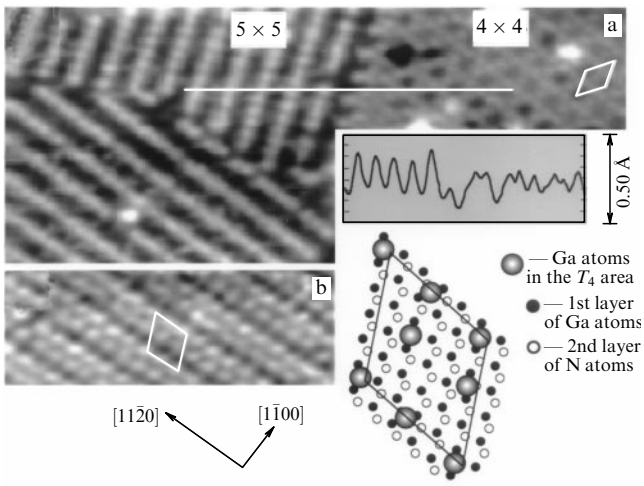

Figure 7. STM images of the occupied states of the 5×5 structural phase: (a) $V_s = -3.0$ V (the scanning profile shows that the difference in contrast between the chains of the 5×5 superstructure and the dots on the 4×4 structure is small, ~ 0.15 Å, and suggests that this is a purely electronic effect rather than a topographical one); (b) $V_s = -2.3$ V [the geometrical model in which several possible positions for adatom relaxation are shown is to the right of figure (b)].

this phase [65, 77], according to which the bright dots in the high-resolution image (Fig. 7b) are related to tunneling from the occupied states of the Ga adatoms, and the observed structure, which is not quite ordered, can be best explained by Peierls lattice distortions of the adatoms located in the T_4 areas. As shown by Peierls [72], in the quasi-one-dimensional case the system may lower its energy by lattice relaxation which leads to formation of a stable semiconducting band structure. In this case, the observed nonuniformity in the position distribution of the atoms along the chain is the result of the relaxation of adatoms occupying positions in the T_4 areas [73], a fact that found its place in the posed model of the 5×5 phase (Fig. 7b). This one-dimensional disorder provides a good explanation for the emergence of strong background in the RHEED patterns, when the electron beam impinges on the sample along the $\langle 1\bar{1}00 \rangle$ direction. Note that the surface coverage in this model amounts to 1.16 monolayers, and the model does not satisfy the electron counting rule [49 – 51].

Later on, it was found that STM images strongly depend on the bias voltage V_s and the tunneling current, a fact subsequently corroborated by Smith et al. [64]. They posed a model in which the irregular distribution of the bright spots is related to the different arrangements of Ga adatoms (in the T_4 areas) and N adatoms (in the H_3 areas), although the experimental conditions employed do not favor such mixing. At the same time, remaining with the Ga-adatom scheme, we cannot point to a single structure with unoccupied dangling Ga bonds that would satisfy the electron counting rule. Taking into account the quasi-one-dimensional nature of the system in question, we believe that here we are dealing with the formation of charge density waves (this name is given to a periodic redistribution of charges in space, which is caused by regular displacements of ions from their equilibrium positions in the crystal lattice) [66], whose generation is related to Peierls distortions [74]. Usually, transitions to states with charge density waves occur in systems with a strong anisotropy of the electron spectrum, an anisotropy realized, in particular, in systems with a chain structure. However, the metallic states in all quasi-one-dimensional configurations prove to be unstable against the formation of collective electronic states, and such transitions lead to the appearance of an energy gap on the Fermi surface accompanied by a loss of metallic properties, so that the electronic spectrum resembles that of an insulator [75]. Here, the quasi-one-dimensional compounds, which found themselves in a state with charge density waves, become insulators, while the metal – insulator phase transition (the Peierls transition) is accompanied by lattice relaxation. In this case, the irregular arrangement of bright spots in the STM image (Fig. 7b) is related to relaxation of the Ga adatoms located in the T_4 areas rather than to the different arrangements of the Ga and N adatoms. If we assume that the average distance 2.5× is the period of this incommensurate lattice along the $\langle 11\bar{2}0 \rangle$ direction, the value of 5× (twice the value of 2.5×) determined from RHEED measurements is the wavelength of a one-dimensional charge density wave, $\lambda = 5a_0$, so that there is no need for the electron counting rule to be satisfied.

Let us now consider the $5\sqrt{3} \times 2\sqrt{13}$ *phase*, which is prepared by depositing 2.0 monolayers of gallium on an as-grown 1×1-Ga surface and annealing the sample for 10 min at 400 °C. The respective STM image (Fig. 8a) made it possible to establish the fact that the structure of this phase is formed by chains consisting of regularly arranged single dots and pairs of dots along the $\langle 11\bar{2}0 \rangle$ direction and that the

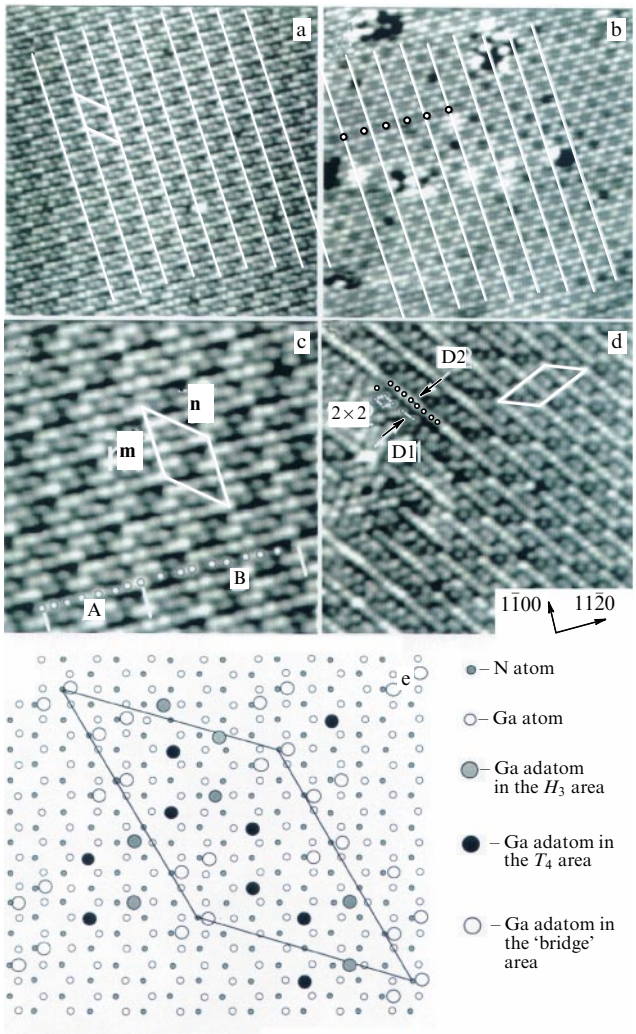

Figure 8. (a) STM image of the occupied states of the surface $5\sqrt{3} \times 2\sqrt{13}$ phase (the white lines are arranged parallel to the $\langle 11\bar{2}0 \rangle$ direction with a period L equal to the projection of vector **n** on this direction, $V_s = -3.0$ V, $I_t = 8 \times 10^{-11}$ A, scanned area is 200 Å × 200 Å). (b) STM image of the 4×4 phase on the same scale as in figure (a) (the small black circles indicate the position of the 4×4 lattice, which means that $5 \times 4a_0 = 4L$, i.e., $L = 5a_0$. (c) Enlarged STM image of the $5\sqrt{3} \times 2\sqrt{13}$ phase (**m** and **n** are the basis vectors of the $5\sqrt{3} \times 2\sqrt{13}$ structure). (d) STM image of the $5\sqrt{3} \times 2\sqrt{13}$ phase demonstrating the transition region. (e) Structural model of the $5\sqrt{3} \times 2\sqrt{13}$ phase, top view (the small light circles represent Ga atoms arranged in accordance with the bulk 1×1 structure; the big light, hatched, and black circles represent Ga adatoms located, respectively, on bridges and in areas H_3 and T_4, and the small black circles represent N atoms of the second layer that are located directly beneath the Ga atoms of the first layer with the 1×1 structure).

chains are 6.4 Å apart (2×). Since the structure in question is fairly complex, to analyze its details we present the image of the 4×4 phase on the same scale (see Fig. 8b). In the enlarged image of the surface (Fig. 8c) we have identified a unit cell with a unit vector **m** along the $\langle 1\bar{1}00 \rangle$ direction. The interchain distance along vector **m** is $\sqrt{3}a_0$, and therefore the size of the unit cell along this direction equals $5\sqrt{3}a_0$. In the direction of vector **n**, the unit cell involves three chains and extends over a distance $5a_0$ along the $\langle 11\bar{2}0 \rangle$ axis (the value was determined by comparing the white lines in Fig. 8a with the line network in the image of the 4×4 phase in Fig. 8b). By comparing these two line networks, one can easily conclude that a four-fold

distance between the lines in Fig. 8a is exactly equal to the five-fold value (63 Å) of the 4× period in Fig. 8b, so that the structure $5\sqrt{3} \times 2\sqrt{13}$ was assigned to this surface.

A distinctive feature of the $5\sqrt{3} \times 2\sqrt{13}$ structure is that it is formed by chains with a one-dimensional unit cell of length $25a_0$ along the $\langle 11\bar{2}0 \rangle$ direction. In turn, each unit cell consists of 16 dots which can be divided into two groups: A (occupying an interval of $10a_0$, which incorporates paired dots at both ends of the interval and four separate dots in between), and B (occupying an interval of $15a_0$, which comprises two pairs of dots and four separate dots), as shown in Fig. 8c. Figure 8d depicts a different domain with a $5\sqrt{3} \times 2\sqrt{13}$ structure rotated through 120 degrees. At the domain boundary one can distinguish points with local 2×2 order (the unit cell is depicted in the same place). In the upper left and lower left corners of the image under examination one can also see linear chains that form a 5×5 structure. If we 'remove' some points, we get a 5×5 structure, and therefore the coverage of the Ga surface with a $5\sqrt{3} \times 2\sqrt{13}$ structure must be close to that of the 2×2 and 5×5 phases. The variations of contrast along the dots in the image of the surface with a $5\sqrt{3} \times 2\sqrt{13}$ structure do not exceed 0.3 Å, which suggests that all the dots are caused by tunneling from the Ga atoms belonging to a common layer.

Our model of this structure is shown in Fig. 8e. Because of the presence of paired dots in the STM images, it is impossible for all bright dots to correspond to atoms occupying regular positions at lattice sites, which means that some Ga atoms might be in different adsorption areas: T_4, H_3, or bridges. However, the theoretical estimates made by Xue et al. [65] and Neugebauer et al. [73] have shown that the presence of Ga atoms in H_3 areas and bridges is disadvantageous energetically. Another possibility is to achieve relaxation of the Ga adatoms occupying the T_4 areas, as in the case of the 5×5 phase. We believe that the 5×5 and $5\sqrt{3} \times 2\sqrt{13}$ phases are two configurations that manifest a unique one-dimensional arrangement of adatoms, which can be explained by the presence of coherent Peierls distortions of the adatom lattice along the $\langle 11\bar{2}0 \rangle$ direction of close packing [72, 74–76]. Furthermore, allowing for the strong dependence of the STM image on the bias voltage and the tunnel current, we believe that within the Ga-adatom scheme the $5\sqrt{3} \times 2\sqrt{13}$ phase will also demonstrate generation of charge density waves at room temperatures but, in contrast to the 5×5 phase, the charge density waves in the $5\sqrt{3} \times 2\sqrt{13}$ structure are commensurate with the surface atomic lattice.

The L-$\sqrt{7} \times \sqrt{7}$ *phase*. This phase exhibits a locally ordered $\sqrt{7} \times \sqrt{7}$ structure and is formed during preparation of the 2×2 phase, provided that the amount of deposited gallium is slightly larger than that needed for the production of the 2×2 or 4×4 phase. Figure 9a gives the typical STM image of the surface with the $\sqrt{7} \times \sqrt{7}$ structure coexisting with the 4×4 phase. Note that we were unable to produce a surface with a single-domain $\sqrt{7} \times \sqrt{7}$ structure by depositing a large amount of gallium or by annealing the sample at other temperatures. Nor were we able to achieve long-range order even when the entire surface was covered by the $\sqrt{7} \times \sqrt{7}$ structure. In all cases we observed a 1×1 RHEED pattern, which meant that local ordering is an internal property of the $\sqrt{7} \times \sqrt{7}$ phase, and for this reason we called it an L-$\sqrt{7} \times \sqrt{7}$ phase. The contrast of the image of the L-$\sqrt{7} \times \sqrt{7}$ phase is higher than that of the neighboring 4×4 phase by no less than 1 Å. In Figure 9b we show our model for this phase, where the hatched circles mark Ga atoms of the adsorbed layer, which are bonded to the 1×1-Ga atoms of the double N–Ga layer.

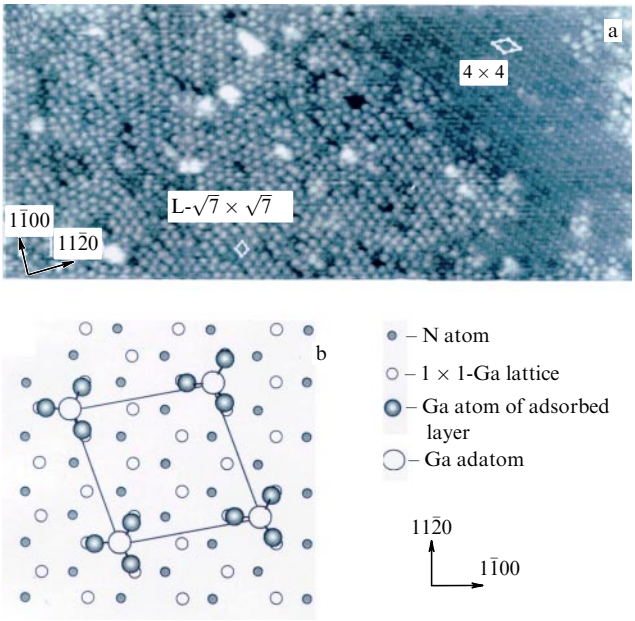

Figure 9. (a) STM image of the GaN(0001) surface containing L-$\sqrt{7} \times \sqrt{7}$ and 4×4 phases (the unit cells are singled out, $V_s = -2.3$ V, and $I_t = 8 \times 10^{-11}$ A). (b) Geometrical model of the surface $\sqrt{7} \times \sqrt{7}$ phase (top view).

The 10×10 *phase*. This phase was produced by additionally depositing 1.5 monolayers of gallium on the L-$\sqrt{7} \times \sqrt{7}$ surface and subjecting the sample to annealing at 350 °C for 10 min. A typical 10×10 reconstruction is shown in Fig. 10a, where it coexists with the L-$\sqrt{7} \times \sqrt{7}$ phase with an image contrast higher than 1.6 Å. According to the preparation conditions, the 10×10 phase contains three Ga layers on the surface with a bulk 1×1 structure (Fig. 10b) and has a unique

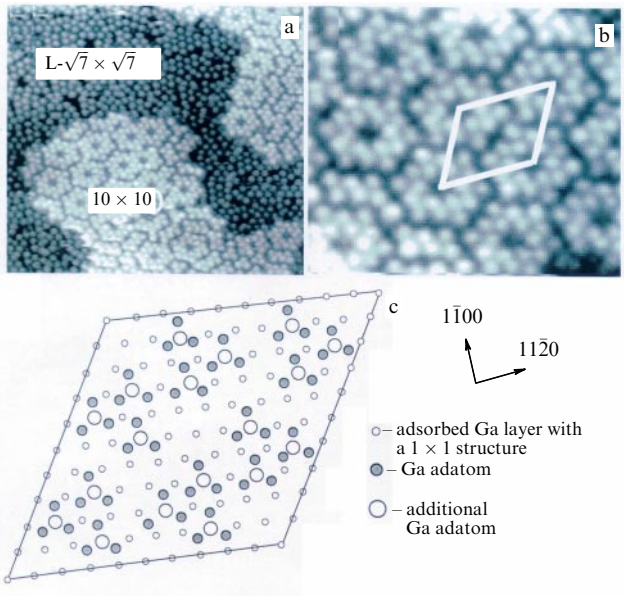

Figure 10. STM images of the occupied states of the structural 10×10 phase: (a) scanned area is 200 Å × 200 Å (the 10×10 phase coexists with the L-$\sqrt{7} \times \sqrt{7}$ phase); (b) enlarged image of the same surface (scanned area is 80 Å × 80 Å; the unit cell is indicated by a white open lozenge), and (c) geometrical model of the 10×10 phase.

honeycomb structure consisting of 18 bright dots in its unit cell (designated by a lozenge): the inner ring contains 6 dots, and the outer ring 12 dots. Many incomplete rings can also be seen in Fig. 10a; these are localized at the edges of an islet with a 10×10 structure. Assuming that energetically the 10×10 phase is more stable than the surface with an L-$\sqrt{7} \times \sqrt{7}$ structure, such local ordering can be interpreted as a phase transition to the 10×10 structure in Ga-enrichment conditions. The atomic model of the 10×10 structure, developed on the basis of an STM image of atomic resolution (Fig. 10b), is depicted in Fig. 10c, where the small white circles designate Ga adatoms residing at the vertices of Ga atoms arranged in such a way that the bulk structure is not changed. The hatched circles represent Ga adatoms bounded with three Ga atoms in the adsorbed gallium layer. In turn, the Ga adatoms of the outer layer (large white circles) are located on these three adatoms (hatched circles).

Irrespective of the polarity of the surface and the conditions needed for phase preparation, all the ordered phases we have so far considered are Ga-enriched phases and can be understood on the basis of the simple Ga-adatom scheme. Notice that neither dimerization nor the absence of atoms at their regular positions in the lattice, which are usually observed on the surface of ordinary semiconducting III – V compounds, is the main mechanism of energy minimization in GaN. What is more, the autocompensation rule, one of the main principles for ordinary semiconducting III – V compounds (GaAs, etc.), cannot always be directly applied to the GaN surface; with the exception of the 2×2 phase, no other phase (including the 4×4 phase) satisfies the electron counting rule. And although the above Ga-adatom model presupposes the existence of a very strong bond in the Ga – N compound, a bond that has a covalent component and an ionic component, electrostatic repulsion between charged adatoms also plays an important role in stabilizing the observed structures. Within this context, the scheme we have presented and the various approaches have proved to be more general and can be applied to other wide bandgap semiconductors.

What is important is that in none of the studies into the phases were traces of formation of dimers/trimers of N or Ga (or their vacancies) discovered, which sets these phases apart from the atomic structures observed on the surfaces of ordinary semiconducting III – V compounds. The formation of III-nitrides generates very high elastic stresses in the films thanks to the substantial difference in the lengths of N – N and Ga – N bonds. In the latter case, the gain in energy proves to be too small to explain the low value of the surface energy, since the length of the Ga – Ga bond on the surface is very close to the Ga – Ga interatomic distance in bulk metallic gallium, and during the association of the Ga atoms in the surface layer the metallic nature of the chemical bond increases even without relaxation. The search for a way to optimize the energy has made it possible to distinguish between two types of reconstruction. The first, to which such phases as 4×4, $2\sqrt{7} \times 2\sqrt{7}$, and 10×10 belong, has a triangular lattice and belongs to the $N \times N$ family. In this case, the leading role is played by the collective interaction between charged adatoms, which leads to formation of Hubbard bands and stabilizes this surface. The second type of reconstructions, which includes the 2×4, 5×2.5, and $5\sqrt{3} \times 2\sqrt{13}$ phases, distinctly demonstrates a quasi-one-dimensional structure, into which atoms that do not belong to the lattice are often included as well. In such phases, a

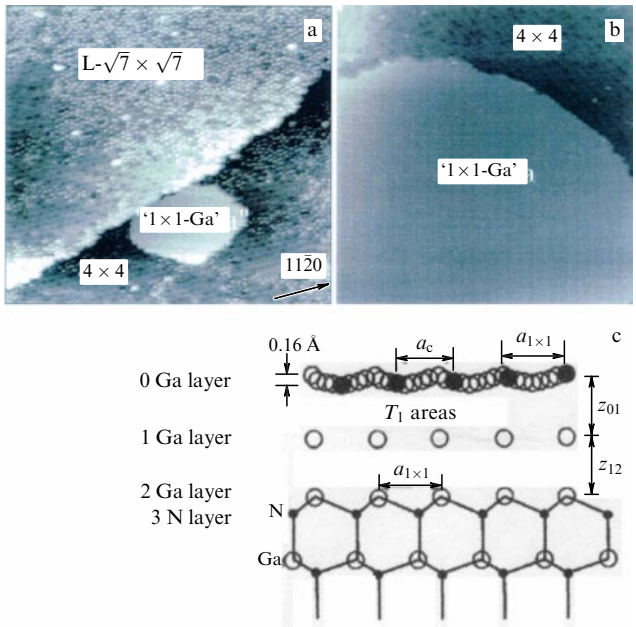

Figure 11. (a) STM image of a GaN(0001) surface demonstrating the coexistence of the 4×4 and L-$\sqrt{7} \times \sqrt{7}$ structures and the pseudo 1×1-Ga fluid phase ($V_s = -3.0$ V, $I_t = 4 \times 10^{-11}$ A, scanning area is 450×360 Å^2). (b) Enlarged image of a 150 Å × 80 Å area of the same surface showing the structure of the pseudo 1×1-Ga fluid phase (the 4×4 phase can be seen in the upper part of the image). (c) The model of a laterally compressed double-layer Ga-coverage on a Ga-enriched GaN(0001) substrate (the average distances between the layers are $z_{12} = 2.54$ Å and $z_{01} = 2.37$ Å, the light and dark circles indicate the positions of Ga atoms at certain instants of time, and the height of the relief of the layer 0 is approximately 0.16 Å [79]).

decrease in the total surface energy can occur because of Peierls distortions of the adatom lattice [65, 72, 74 – 76].

The last observation in this series is that of the *pseudo* 1×1-Ga *fluid phase* (Fig. 11). This phase is Ga-enriched to the highest degree and always coexists with other surface structures, except for the 1×1 surface of an as-grown GaN film. Figures 11a and b show the STM images taken in the process of preparing a 2×2 surface. The coexisting 4×4, L-$\sqrt{7} \times \sqrt{7}$, and pseudo 1×1-Ga phases are also shown. The pseudo 1×1-Ga fluid phase was first discovered by Smith et al. [78]; its structure differs dramatically from that of an as-grown 1×1 surface and, as shown by STM images, is probably close to the structure of a bulk GaN. At the same time, the RHEED patterns obtained at temperatures lower than 350 °C reveal the presence of additional reflections, which suggests that the basis vectors of the surface unit cell are much longer than the basis vectors of the 1×1 unit cell, while the analysis of the Auger spectra pointed to the presence in the pseudo 1×1-Ga phase of 2 to 3 monolayers of Ga above the double Ga – N layer [78]. Northrup et al. [70] posed a model for this phase. The researchers assumed that the pseudo 1×1-Ga surface is a laterally compressed incommensurate double-layer structure (Fig. 11c). The corrugated potential relief observed in STM images is the result of time averaging, which is included in STM sampling procedure. It is assumed that the Ga atoms on the surface appear to be ordered enough for additional reflections to emerge in the RHEED patterns, but at the same time they are relatively mobile for the time-averaged corrugated relief (caused by the motion of Ga atoms over the substrate with the 1×1

structure) to appear in STM images. In Fig. 11b, the surface of the pseudo 1×1-Ga fluid phase appears to be atomically smooth. Not with one of the STM images of this phase were we able to achieve higher resolution. Measurements of the scanning profiles showed that this phase is higher than the 4×4 structure by 2.1 Å. According to the theoretical model proposed by Fritsch et al. [59], the surface 2×2 phase is higher than the bulk 1×1-Ga layer by 1.78 Å, with the result that the height of an islet with a pseudo 1×1-Ga structure exceeds that of the bulk 1×1-Ga layer by 3.88 Å, which corresponds to a 1.9-monolayer coverage.

The surface with a pseudo 1×1-Ga structure always manifested its metallic nature, since tunneling proved to be stable even at bias voltages $V_s \leqslant 0.2$ V, and STM images obtained with low bias voltages were similar to those obtained with high bias voltages. The size of the regions of a surface with the pseudo 1×1-Ga structure reached several thousand angströms. Even if we assume that such a surface had been nitridized at 500 °C, we still did not notice any changes, and only the edges of islets with a pseudo 1×1-Ga structure became brighter. In contrast to this, all other structures disappeared completely after such a treatment. Our observations clearly suggest that the pseudo 1×1-Ga fluid phase is extremely stable and remains so as long as the surface is Ga-enriched. This presupposes an extremely low solubility of nitrogen in bulk gallium and is in good agreement with the model of a laterally compressed double Ga layer, proposed by Northrup et al. [79]. Note that for the surface to have a plain morphology, the material must be grown in Ga-enrichment conditions.

4.3 Growing N-polar GaN thin films and atomic structures on the GaN(000$\bar{1}$) surface

In contrast to Ga-polar epitaxial films grown on sapphire by the MOCVD technique, N-polar films were always very coarse and had a higher defect density [15]. However, the use of high-quality SiC substrates has made it possible to believe that the quality of GaN films with N polarity can be raised. In Section 4.1 we noted that GaN films grown on Si-polar 6*H*-SiC substrates are Ga-polar, so we can expect the films grown on C-polar substrates to be N-polar.

Growth and polarity of thin GaN(000$\bar{1}$) *films*. The 6*H*-SiC(000$\bar{1}$) substrates were cleaned by etching in an Si flux in an ultrahigh vacuum. After that, a buffer AlN or GaN layer about 100 Å thick was deposited at 550 – 600 °C, the substrate temperature was raised to 700 °C, and the process of growing GaN films was begun. The growth was stopped by quenching the nitrogen plasma, after which 2 monolayers of Ga were deposited on the film at the same temperature. Growing the film in the course of 2 h in Ga-enrichment conditions, we produced GaN films up to 3500 Å in thickness, and Ga flux was kept at such a level that the growing film produced a distinct 1×1 RHEED pattern (Fig. 12a), which suggested a two-dimensional growth mode. If an additional amount of Ga was deposited on the surface and the sample was subjected to low-temperature (250 – 350 °C) annealing, then, depending on the Ga coverage, a series of ordered structures, such as 2×3, 2×4, $\sqrt{7} \times \sqrt{7}$, $2\sqrt{7} \times 2\sqrt{7}$, 6×6, and 6×8, could be produced. An example of such ordering is presented in Fig. 12b, which shows a RHEED pattern corresponding to the 6×6 reconstruction.

Although the substrate surface was atomically smooth and the RHEED patterns on the epitaxial GaN(000$\bar{1}$) film were striped, the AFM image in Fig. 12c clearly demonstrates that on the whole the morphology of the surface of an N_1-polar GaN film is not as flat and homogeneous as the substrate and that on it there is a characteristic *mesa structure* in the form of irregularly shaped isolated cusps with flat tops 50 – 100-Å high and twisted boundaries between them. Note that in the AFM images of Ga-polar films grown on SiC(0001) substrates the surface appeared to be smooth and structureless [34, 35], which presupposes a higher lateral growth rate. STM measurements taken on the tops of the cusps revealed the presence of a terrace – step structure (Fig. 12d), with alternating single or double steps (whose height was equal to that of a double-layer Ga – N coverage) observed along the major crystallographic directions. Similar results were obtained by Xie et al. [80]. The researchers assumed that there are two types of steps: type A steps consisting of edge atoms with two dangling bonds, and B-steps consisting of atoms with one dangling bond. Thus, the more active type A steps grow faster and are captured by type B steps of the underlying layer, which results in the formation of steps whose height is equal to the thickness of double-layer Ga – N coverage (i.e., in grouping of steps), as shown in Fig. 12d. Bearing in mind that no formation of islets was observed in the terraces, we conclude that such anisotropic growth behavior is proof of the two-dimensional mode of step growth and agrees with the RHEED data.

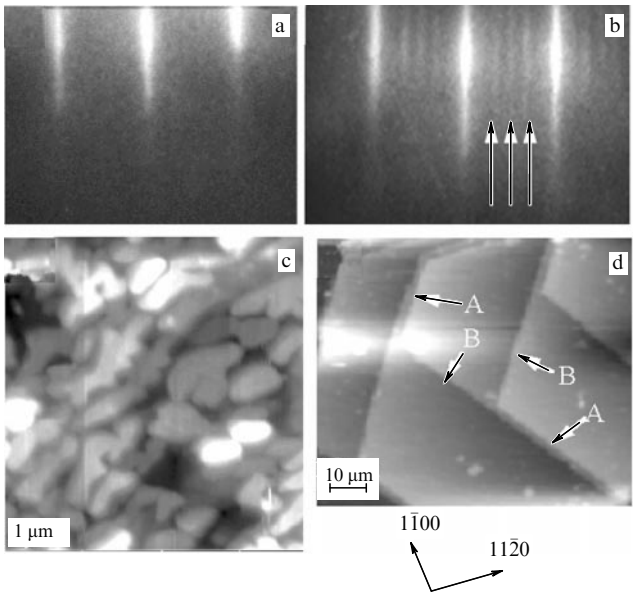

Figure 12. RHEED patterns along the azimuthal ⟨11$\bar{1}$2$\bar{1}$⟩ direction on a GaN(000$\bar{1}$) film: (a) with an as-grown 1×1 surface; (b) with a 6×6 reconstruction produced after depositing gallium and subsequent annealing; (c) AFM image of the same film demonstrating a mesa, and (d) STM image of the surface of cusps on the film (the arrows point to steps of A and B types, $V_s = -2.7$ V, and $I_t = 1 \times 10^{-11}$ A).

Figure 13a illustrates the STM image of the occupied states for the 6×6 reconstruction corresponding to the RHEED pattern in Fig. 12b. Its ringlike structure is the same as that observed by Feenstra's group (see Ref. [46]) on the GaN(000$\bar{1}$) surface, whose N polarity was established beforehand; the last circumstance means that our films were also N-polar. On the other hand, on the epitaxial GaN films grown on the Si-polar 6*H*-SiC(0001) surface, which we decided are Ga-polar, we observed a series of reconstructions 2×2, 4×4, 5×5, $5\sqrt{3} \times 2\sqrt{13}$, $\sqrt{7} \times \sqrt{7}$, and 10×10 (see

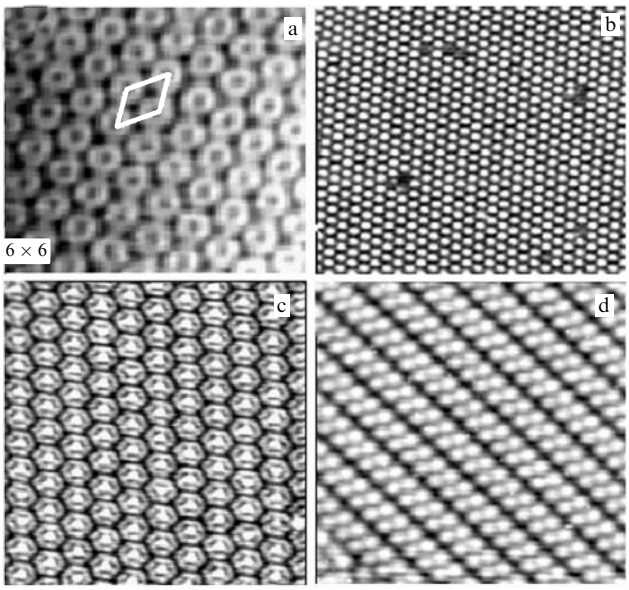

Figure 13. STM images of atomic structures on the GaN(000$\bar{1}$) surface: (a) 6×6 phase (the unit cell is indicated by a white open lozenge, $V_s = -2.7$ V); (b) $2\sqrt{7} \times 2\sqrt{7}$ phase ($V_s = -2.7$ V); (c) $2\sqrt{7} \times 2\sqrt{7}$ phase ($V_s = 2.7$ V), and (d) 2×4 phase ($V_s = -2.7$ V).

Section 4.2), which agrees with the data obtained by the same group for a Ga-polar surface [47]. What finally determined the polarity of the films was the result of etching in KOH, which leads to rapid dissolution of the films (the evolution of the surface morphology was monitored by an AFM). It also agrees with the chemical properties of N-polar GaN films [51]. Thus, wurtzite GaN films grown on the 6*H*-SiC(000$\bar{1}$) surface are N-polar, while those grown on the 6*H*-SiC(0001) surface are Ga-polar. This coincides perfectly with Hellman's conclusions [15] and can be attributed to the strong ionicity of GaN and SiC compounds [81–83].

The atomic structures on the surface of GaN(000$\bar{1}$) films grown on sapphire by the MBE technique were first studied by Smith et al. [46–48]. The GaN films we grew on SiC(000$\bar{1}$) substrates with an AlN buffer layer usually reveal a 1×1 RHEED pattern, while additional Ga coverage with subsequent annealing led to the appearance of Ga-stabilized surface phases whose atomic structures were established on the basis of STM images and the results of *ab initio* total energy calculations. For instance, the $2\sqrt{7} \times 2\sqrt{7}$ reconstruction (Figs 13b and c) was produced by depositing 3 to 4 monolayers of Ga on the Ga-1×1 surface at 200 °C and subsequently annealing the sample at the same temperature over the course of 10 min. The RHEED pattern along the $\langle 11\bar{2}0 \rangle$ direction had two strips of reflections of fractional order, localized near the center of the zeroth Laue zone. As this was warmed up to 600 °C, a transition to the 2×4 structure was recorded (Fig. 13d). Figure 13b shows an STM image of the unoccupied states for the $2\sqrt{7} \times 2\sqrt{7}$ reconstruction, which at a bias voltage $V_s = 2.8$ V appears to be a hexagonal array of large rounded maxima. If we connect the centers of the nearest maxima, we get the unit cell of this phase. As the bias voltage V_s was reduced to 1.5 V, each maxima transformed into a hexagonal ringlike structure, while at $V_s = 0.6$ V the maximum at the center of the ringlike structure manifested itself in the form of a hole. The STM images of the occupied states for the $2\sqrt{7} \times 2\sqrt{7}$ reconstruction (Fig. 13c) also exhibited a dependence on the bias voltage, and at $V_s = -2.8$ V the image consisted of hexagonal rings, with a triangular structure at the center of each ring (this structure intersects the ring's edge at an angle of 120 degrees). The image of the atomic structure of the surface suggests that the vectors of the unit cell are turned away from the direction of close packing, and its $2\sqrt{7} \times 2\sqrt{7}$ symmetry is identified by comparing with a 2×4 reconstruction of the same size (Fig. 13d). Note also that all STM images were obtained by using the same scanning probe in stable vacuum conditions and on the same terrace, with the dependence on the bias voltage distinctly reproduced for each surface with a $2\sqrt{7} \times 2\sqrt{7}$ structure. The last circumstance means that observed changes in the images are caused not by the probe-tip we used (no tip effect) but correspond to the local density of states at different energy levels.

Figure 14 shows high-resolution dual-mode STM images of the $2\sqrt{7} \times 2\sqrt{7}$ reconstruction (Fig. 14a) and the 6×8 reconstruction (Fig. 14b) (in this mode, an alternating positive and negative bias voltage V_s is applied). The upper halves in Fig. 14a and b are the images of the occupied states obtained at $V_s = -3.0$ V, and the lower halves are the unoccupied-state images ($V_s = 3.0$ V) of the same area of the surface. Obviously, the $2\sqrt{7} \times 2\sqrt{7}$ and 6×8 superstructures manifest themselves differently in both cases, although both the image (a) and image (b) show the same symmetry and distinct correlation. For instance, the large bright cusps in the image of unoccupied states of the $2\sqrt{7} \times 2\sqrt{7}$ reconstruction correspond to a hexagonal ringlike structure with six maxima in the occupied-state image. However, the center of a ringlike structure in the occupied-state image is displayed differently: for $V_s < 0$ it manifests

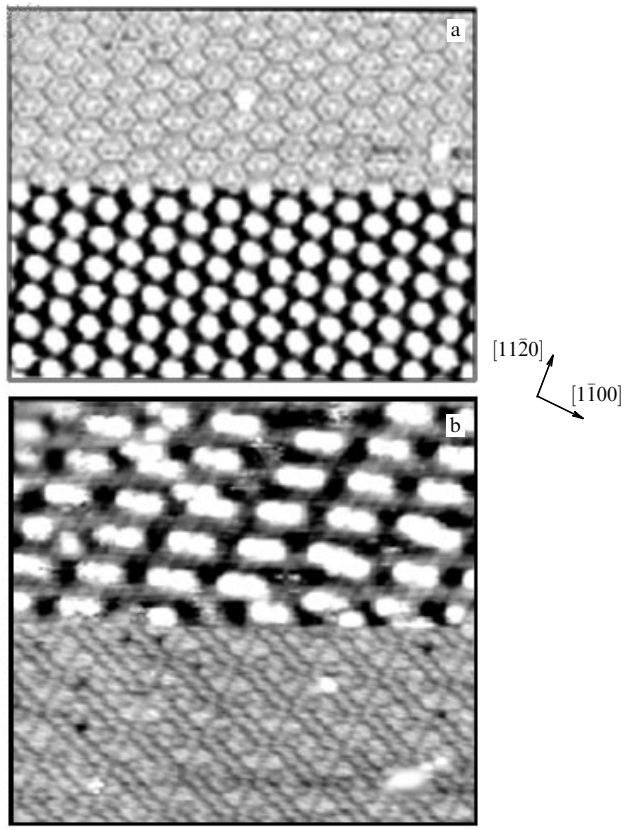

Figure 14. Dual-mode images of the GaN(000$\bar{1}$) surface: (a) $2\sqrt{7} \times 2\sqrt{7}$ reconstruction, and (b) 6×8 reconstruction.

itself in the form of lower cusps, while for $V_s > 0$ it is a bright cusp positioned above the hexagonal ring. Thus, the images of both occupied and unoccupied states of the $2\sqrt{7} \times 2\sqrt{7}$ reconstruction demonstrate a strong dependence on the bias voltage, which suggests that the surface is semiconducting and contains a large number of surface electronic states.

Let us return to the Ga-polar GaN surface. Notice that further exposure of the surface of Ga-polar films to nitrogen plasma did not lead to the appearance of nitrogen-induced ordered structures. The resulting surface always turned out to be coarse and disordered, and no terraces were discovered in the STM images. This could be due to the lower mobility of nitrogen adatoms on a Ga-polar surface [86], which hinders the search for equilibrium positions. To reduce the number of dangling bonds at the surface in N-enrichment conditions, the nitrogen adatoms on the growing surface could have formed new bonds, for instance, by dimerization. However, in view of the high binding energy of the atoms in a nitrogen molecule (≈ 5 eV), these bonds prove to be thermodynamically unstable under evaporation in the form of N_2 molecules [73], so that the nitrogen atoms from the first layer have no way to form dimers as stable structures on the surface — they will evaporate largely in the form of N_2 molecules. If such dimers are formed, they appear only as a transient phase preceding the formation of N_2 molecules, and with a very low activation energy. This is also the reason for the large difference between the equilibrium concentration of nitrogen atoms and the equilibrium concentration of gallium atoms on the GaN surface. Hence, although the growth took place in nitrogen-enrichment conditions, the growing surface may have experienced a local deficit of nitrogen atoms, which limited the kinetics of formation of N-enriched structures, theoretically predicted in Refs [73, 84]. Besides, because of the very short N – N bond (1.8 Å) in the N_2 molecule compared to the surface GaN lattice constant (3.2 Å), the process of nitrogen dimer formation involves large distortions in the bonds, generates elastic stresses in the film, and hence leads to a large expenditure of energy, which may be one of the reasons for the difficulties in growing III-nitride films. To increase the number of nitrogen atoms introduced into the growing layer and decrease the concentration of nitrogen vacancies which are usually present in III-nitride films, one must run the growth process in conditions of nitrogen enrichment. However, this is usually difficult to achieve with the MBE technique. In this case, the growth kinetics can be controlled by adding surfactants or by changing the surface free energy [73, 85]. The last circumstance also explains why the MBE technique has proved less effective in growing III-nitride films than the MOCVD method where hydrogen may act as the surfactant.

On the other hand, in conditions of enrichment in Ga with a stably growing surface and with allowance for a much larger diffusion coefficient of gallium atoms, it is quite natural to expect the formation of a plain morphology of the GaN surface [73, 84 – 86]. In Section 4.2 we noted that in conditions of very intense enrichment with Ga there may form a mobile atomically flat pseudo 1×1-Ga fluid phase, which smooths the inhomogeneities that appear on the surface. Such a behavior differs dramatically from the one that occurs on the surface of common semiconducting III – V compounds. For instance, in the case of epitaxial growth of GaAs, to produce a high-quality film with a plain morphology one must always have an excess of As [27]. On the other hand, film growth in the conditions of Ga enrichment may result in the formation of Ga clusters and even Ga droplets [87], which may lead to the emergence of nonstoichiometric coverages and coarsening of the surface and hinder the production of high-quality GaAs films. Thus, the kinetic processes in the course of the MBE growth of III-nitride films differ substantially from those that occur in the case of common III – V compounds. At the same time, the analysis of STM images of the GaN surface discovered no Ga-dimer formation. The reason may be that the distance between the nearest Ga – Ga neighbors in bulk gallium is very close to the bond length in Ga dimers, and the gain in energy because of dimer formation is insignificant. At the same time, on the GaN(0001) surface with tetrahedral bonds [the structure of this surface is similar to that of the (111) surface of cubic GaN and is characterized by three-fold symmetry], the dangling bonds of 1×1-Ga are aligned parallel to the normal to the surface, and therefore the restrictions on dimerization prove to be more important than for the (001) surface of cubic GaN. For this reason, we attributed the characteristic features in the images of this surface to tunneling from Ga adatoms, and within this scheme it was easy to recognize that the number of surface reconstructions that satisfy the electron counting rule is limited.

The above 2×4 and $2\sqrt{7} \times 2\sqrt{7}$ reconstructions, as well as the results of Smith et al. [46 – 48], were obtained by depositing an additional amount of Ga atoms on the assumption that the gallium atoms on the GaN(000$\bar{1}$) surface possess a higher mobility with a lower diffusion barrier and easily find their equilibrium positions. All this is in good agreement with the results of the theoretical studies by Visconti et al. [83] and explains why high-quality films with a plain morphology are always produced in conditions of gallium enrichment. The same is true of the GaN(0001) surface [5, 14].

5. Epitaxial growth of GaN thin films on GaAs(001)

Cubic GaN has a number of advantages in the fabrication of electronic devices: a higher crystallographic symmetry, a smaller effective electron mass, and higher ballistic velocities of electrons due to weaker phonon scattering [8, 89]. As noted earlier (see Section 2), because of the absence of suitable substrates and the metastable nature of cubic GaN, the fabrication of high-quality films of cubic GaN constitutes a difficult task. The nonequilibrium growth technologies, MBE in particular, make it possible to produce β-GaN at relatively low temperatures, and the optimal substrate for epitaxial growth from the viewpoint of lattice mismatch and thermal expansion is 3*C*-SiC. Thanks to their metastable properties, cubic GaN films often contain the thermodynamically stable wurtzite phase. For instance, insufficient or excessive nitridation of the widely used GaAs(001) substrate in the initial stage of growth leads, in the final analysis, to formation of hexagonal GaN [22]. When a 3*C*-SiC(001) substrate is utilized, the film growth proves to be less susceptible to nitridation, but the film's quality strongly depends on the crystallinity and morphology of the substrate, as well as on the concentration ratio [N]/[Ga] in the fluxes [88].

The atomic structures on the cubic GaN(001) surface have been studied mainly by the RHEED method. The 2×2 and $c(2 \times 2)$ structures were observed on the surface of β-GaN grown on the GaAs(001) substrate [22, 89, 90], while the 4×1 structure was observed on the surface of β-GaN grown on the

3*C*-SiC(001) substrate [22, 91]. These phases guarantee a stable growth front of the GaN film and make it possible to monitor the stoichiometry of the surface by RHEED control of the surface structure. In order to better understand the properties of cubic GaN, we did *in situ* STM studies of the epitaxial growth of GaN films on the GaAs(001) substrate, including studies of the effect of various surface nitridation modes on the growth of GaN films.

5.1 Nitridation of the GaAs(001) surface

The preparation of GaAs(001) samples and the growing of homoepitaxial GaAs(001)-2 × 4 films have been described in our earlier review (see Ref. [27]). The heteroepitaxial growth of the GaN/GaAs(001) system must take into account both the lattice mismatch (up to 20%) and the substantial difference in the thermal expansion coefficients. After the buffer GaAs layer had been grown (a distinct 2 × 4 RHEED pattern could be seen on it) and annealed in an As flux, the sample was exposed to a flux of nitrogen plasma at a substrate temperature of 500 °C. The evolution of surface structure as the sample was exposed to the plasma and the changes in the substrate temperature were controlled by the RHEED method. The sample was then studied by an STM.

The 2 × 4 *surface*. Most research in the nitridation of the GaAs(001) substrate has been conducted on As-enriched GaAs(001) surfaces containing large 2 × 4 terraces separated by double-layer steps 2.8 Å high. Two types of steps are prominent on such surfaces: type A steps with straight edges oriented along the $\langle\bar{1}10\rangle$ direction, and bent steps of type B oriented along the $\langle 110\rangle$ direction [27, 92, 93]. The first to successfully observe the nitridation of the GaAs(001)-2 × 4 surface by the STM method were Gwo et al. [94]. They were also the first to observe a 3 × 3 reconstruction and proposed a nitrogen dimer model to explain it. However, Bykhovski and Shur [95] found that the process of formation of nitrogen dimers on the GaAs surface is unstable due to the very small covalent radius of nitrogen compared to that of gallium and that the resulting distortions of the bond generate large elastic stresses in the layer, so that the very existence of a nitrogen dimer is doubtful.

After nitridation at 500 °C, the terrace – step structure was still quite obvious in the STM images. This suggests that the changes in the morphology of the surface layer were very small compared to those in the morphology of the substrate and that an atomically smooth nitridized surface was formed. However, anisotropic vacancy islets elongated along the $\langle\bar{1}10\rangle$ direction can be seen to appear on the terraces, while the edges of type A steps become irregular. It is possible that these changes are caused by preferential etching of the steps by nitrogen atoms, and the anisotropy of the shape of the vacancy islets is related to the preferential etching of type B steps, since the separation energy from type B steps is lower [92]. In addition to the large vacancy islets, some smaller islets (several angströms in perpendicular directions) shaped almost evenly were also observed, although these were not defects of the type of absent atoms on the starting 2 × 4 surface, where their size does not exceed 10 Å. Most probably these small islets appear because of random etching of terraces, but because of the continuing effect of nitrogen plasma they finally develop into anisotropic vacancy islets. This provides a natural explanation for the observed change in the morphology of the surface layers and is in good agreement with the substrate coarsening model proposed by Okumura et al. [22]. At the same time, the 2 × 4 structure of dimer rows proved to be replaced by a layer consisting of small bright dots arranged with a periodicity of 3× along the $\langle\bar{1}10\rangle$ direction. Along the $\langle 110\rangle$ direction, the arrangement of these dots was not so regular, which led to the appearance of twisted lines in the image of the surface. Nevertheless, the arrangement of dots with 3× spacings was preferential, and there were also a small number of locally ordered domains with a 3 × 3 structure. We called this structure a 'distorted' 3 × 3 phase.

The 2 × 6 *surface*. Trampert et al. [93] produced an As-enriched 2 × 6 surface by annealing an As-enriched 2 × 4 surface without placing the sample in an As flux. Figure 15 shows the STM images obtained after nitridation for different times of exposure. As in the previous case, the surface is atomically flat and one can observe a terrace – step structure on it, which suggests that a homogeneously nitridized layer has been formed. The terraces also exhibit a large number of vacancy islets, whose size grows along the $\langle\bar{1}10\rangle$ direction as the time of exposure increases. At the same time, although after nitridation the surface does consist of regular arrays of small dots, the analysis of its structure made it possible to detect the presence of two characteristic features that had not been observed on the 2 × 4 surface, namely, domains with a 3 × 3 structure that are well-ordered and exhibit 3× translational symmetry along the principal crystallographic axes (see the inset to Fig. 15c), and bright lines that separate these domains; these lines proved to be fairly stable in the course of further nitridation and subsequent annealing. As the time of annealing in an ultrahigh vacuum grows, desorption of the 3 × 3 structure begins, the rows of As dimers become more and more prominent, and finally the 2 × 6 structure is restored. Measurements of the scanning profiles have shown that the bright lines are 0.60 ± 1.15 Å above the 3 × 3 spots, which suggests that these lines correspond to As dimers with a 2 × 6 structure.

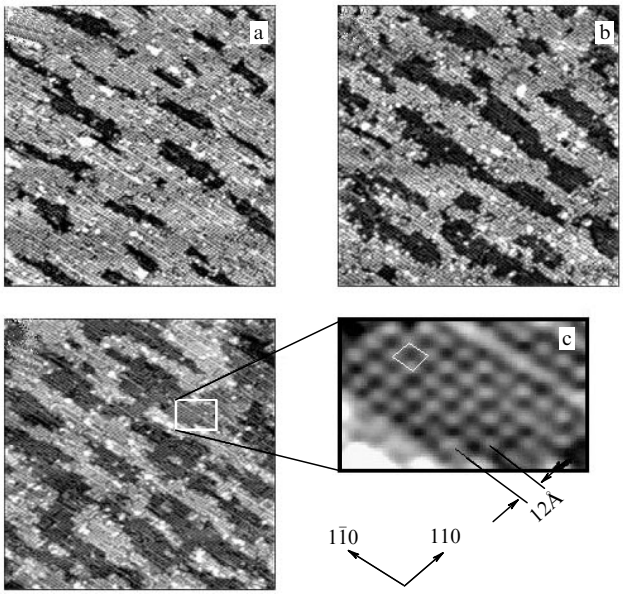

Figure 15. STM images of the As-enriched surface of GaAs with a 2 × 6 structure after nitridation at 550 °C that show the evolution of the surface morphology and the etching process in a nitrogen plasma for different times of exposure: (a) 5 s; (b) 10 s, and (c) 17 s; $V_s = -3.3$ V, $I_t = 4 \times 10^{-11}$ A, and the scanned area is 1000 × 1000 Å^2. The inset gives the enlarged image of a section of the surface with a 3 × 3 structure.

The higher degree of ordering of the nitridized 3×3 layer on a surface with a 2×6 structure and the stability, which to a great extent is inherent in the 2×6-As structure, strongly affect the quality of the GaN film grown. For instance, not so long ago, Trampert et al. [93] studied the cross section of samples with a transmission electron microscope. The researchers reported on growing a high-quality cubic GaN film, an achievement attributed to the existence of what is known as the 'magic mismatch' of GaN and GaAs lattices: $5a_0(\mathrm{GaN}) = 4a_0(\mathrm{GaAs})$. On the reconstructed 2×6 surface, such coincidence occurs along the $\langle 110 \rangle$ direction, where the five-fold periodicity of the $3\times$ lattice of GaN is almost exactly equal to the two-fold periodicity of the $6\times$ lattice of GaAs. If nitridation proceeds by the simple $\mathrm{N} \leftrightarrow \mathrm{As}$ exchange mechanism, the corresponding symmetry of the $6\times$ substrate provides a natural template for the ordering of $3\times$. But complete ordering leads to a transformation of the stress field in the nitridized layers and may require switching on the mechanism of stress lifting, e.g., by creating defects and/or elastic relaxation. If necessary, they may become centers of crystallization and formation of edge dislocations during the subsequent growth of the films, as observed by Trampert et al. [93]. However, in view of the simultaneous etching of the terraces, it is difficult to decide whether or not such a process is limited kinetically.

The ordering of $3\times$ along the direction of substrate dimerization and the formation of a completed nitride layer assume that the structure is coherently stressed with the substrate. But, irrespective of how the N atoms are bonded to the underlying Ga layer, the observed commensurability is the basic cause of stresses in the surface layer. Lifting/reducing the elastic stresses may manifest itself even in a single-layer GaN due to defect formation at the interphase boundary, the formation of three-dimensional islets, and the coarsening of the surface [22]. Assuming that the nitridation is done by the simple $\mathrm{N} \leftrightarrow \mathrm{As}$ exchange mechanism, and taking into account the correlation between the ordering of the substrate and the distortion of the 3×3 structure, we conclude that the irregular distribution of spots is an indicator that deformation of local bonds has lifted the stresses.

Additional nitridation of the GaAs(001) *surface*. As noted earlier, short-duration ($\sim$ 10 s) nitridation of the GaAs(001)-$2 \times 4/2 \times 6$ surface at a relatively low temperature ($\sim$ 500 °C) leads to formation of a coherently stressed GaN thin layer with a plain surface morphology and a local 3×3 ordering. But if the duration of nitridation exceeds 60 s, the surface morphology coarsens substantially. Images obtained after 60 s of exposure to a nitrogen plasma showed that three-dimensional GaN crystallites 40 – 50 Å in height and 200 Å-by-300 Å in size appear on the surface near the edges of steps, while disordered domains with a 3×3 structure can be observed on the part of the surface not covered with islets. Most probably, because of nitridation of the second layer of As subjected to the action of gallium, Ga atoms migrate to the edges of steps to form GaN. Accordingly, if the sample temperature it too high, the surface produced as a result of nitridation also proves to be very coarse.

5.2 Epitaxial growth of GaN thin films on GaAs (001)

In this case, after the buffer GaAs layer with a distinct $2 \times 4/2 \times 6$ RHEED pattern had been grown, the sample was exposed to a nitrogen plasma for a period so long that a transition from the $2 \times 4/2 \times 6$ structure to a nitrogen-induced 3×3 superstructure took place. Usually, about 10 s of exposure was enough for the 3×3 reflections to fully manifest themselves and reach their maximum intensity; as nitridation continued, these reflections became weaker and weaker and finally transformed into a spotted 1×1 pattern.

Growth with short-duration nitridation. This was begun at the moment when the distinct 3×3 RHEED pattern had fully developed; subsequent optimization of the growth conditions led to the formation of single-crystal cubic GaN. As the buffer layer grew, the RHEED pattern gradually transformed from the distinct 3×3 to the spotted 1×1, which meant that three-dimensional GaN islets were forming on the GaAs(001) surface. At this stage, the growth occurs under conditions of strong nitrogen enrichment; studies involving a transmission electron microscope favored the view that in this case well-oriented GaN crystallization centers epitaxially bonded to the substrate appear at the initial stage [96, 97]. After the low-temperature buffer layer had been grown, the substrate temperature was increased to 670 °C and the concentration ratio [N]/[Ga] was decreased almost to unity, so that the basic film could begin to grow. As the film grew, the RHEED patterns retained their cubic symmetry. After roughly 1 h of growing the film ($\geqslant$ 1000 Å) the reflections became elongated and thin, and weak 2×2 strips became visible. The STM image of such a film (Fig. 16a) clearly shows a terrace – step structure, with the step height being 2.26 Å (see the arrow), which corresponds to a double-layer step of cubic GaN. The high-resolution image in Fig. 16b bears witness to reconstruction of the 2×2 surface (the unit 6.4 Å-by-6.4 Å cell is singled out). Earlier, Amano et al. [9] and Trampert et al. [21] reported on a 2×2 reconstruction on the surface of cubic GaN grown on GaAs(001), while additional deposition of gallium led to a $2 \times 2 \rightarrow \mathrm{c}(2 \times 2)$ transition. These two

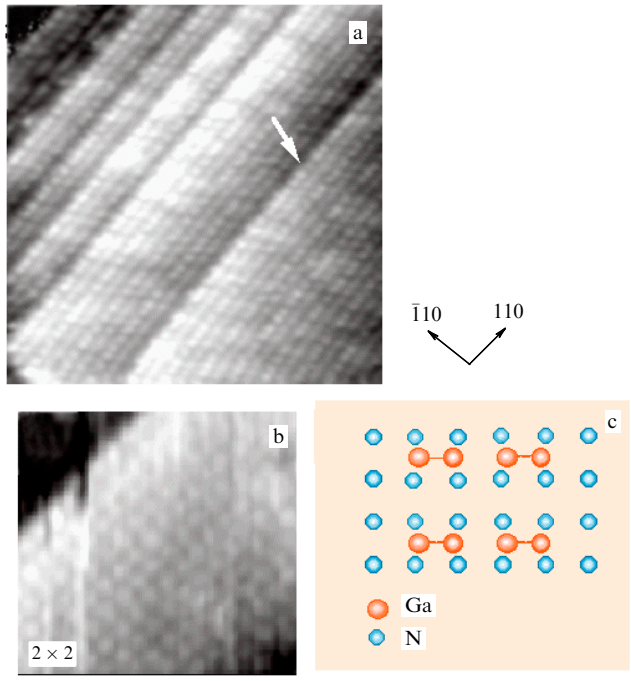

Figure 16. Occupied-state STM images of the surface of cubic GaN: (a) scanned area is 250×250 Å^2 (the arrow points to a single step of double-layer GaN); (b) scanned area is 80×80 Å^2 (the unit 2×2 cell is singled out), and (c) a model of a 2×2 reconstruction (Ga atoms of the upper layer form Ga – Ga dimers along the $\langle 1\bar{1}0 \rangle$ direction).

superstructures were produced by depositing additional gallium on a 1×1 surface which was assumed to be N-polar. Since we used similar growth conditions, our structure was also a 2×2 structure, and the cusps in the occupied-state STM image (Fig. 16b) are formed because of tunneling from gallium atoms. Each atom of the upper layer of a section of GaN with the bulk structure has two dangling bonds, with the result that the dimerization of atoms on the surface is advantageous energetically. Our model of the 2×2 reconstruction, which is based on the Ga – Ga dimer structure, is presented in Fig. 16c. Two neighboring Ga atoms of the upper layer form a dimer along the $\langle \bar{1}10 \rangle$ direction, and they are bonded to four N atoms of the second layer.

Growth with long-duration nitridation. This growth, which leads to the formation of GaN islets, took a different course. RHEED showed a spotted pattern during the entire growth process, and changes in the [N]/[Ga] ratio did not affect the surface morphology, which indicates that the growth mode was three-dimensional. Moreover, the RHEED pattern exhibited additional diffraction spots which were related to the cubic phase and originated in the hexagonal grains in the film (it is assumed that the cubic and hexagonal phases coexist in the given film). Large-area STM images exhibited a coarse surface morphology, and in some case there were flat terraces with a $2\sqrt{7} \times 2\sqrt{7}$ reconstruction, for which the strong dependence on the bias voltage is a characteristic feature (see Fig. 14). Such a structure was observed in GaN films grown on a SiC(000$\bar{1}$) substrate, and subsequently indicated that a hexagonal GaN phase was being formed.

As mentioned in Section 1, GaN crystals, either with the wurtzite structure or with the zinc blende structure, consist of tetrahedral matched unit cells with a cation at the center and an anion at the edge, or vice versa. The only structural difference is that the direction of closest packing is $\langle 111 \rangle$ for cubic GaN, and $\langle 0001 \rangle$ for wurtzite GaN. The defect in the sequence of arrangement (the stacking fault) transforms one structure into the other. Figure 17 schematically illustrates the transition from cubic GaN(111) to wurtzite GaN(0001), where the dashed line stands for the (111) plane which is the stacking fault. Since the cubic GaN is metastable and the difference in energy between the cubic and wurtzite phases amounts to only 9.8 meV per atom [98], the facets (111) of a three-dimensional nucleus of cubic GaN may become the nucleation centers for a thermodynamically stable hexagonal phase. This is why epitaxial GaN films whose growth began after prolonged nitridation (which leads to a three-dimensional growth mode) contained mixed cubic and hexagonal phases.

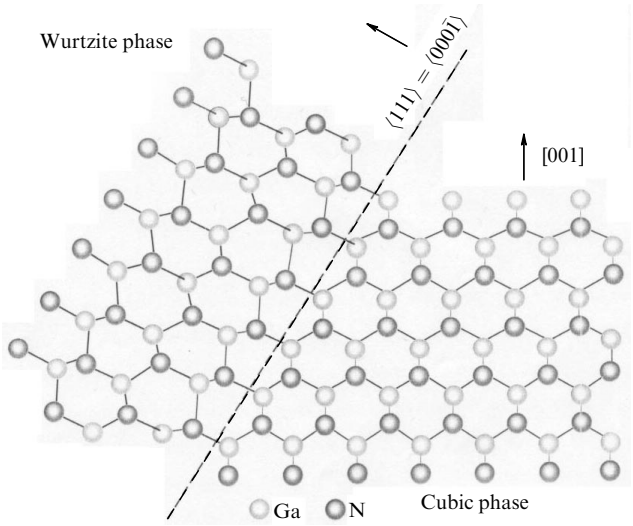

Figure 17. Coexistence of the stable wurtzite phase and the metastable cubic phase in a GaN film. (The boundary separating the cubic phase from the wurtzite phase is shown by a dashed line.)

Optimization of the growth conditions plays an important role in suppressing the formation of the hexagonal phase in a cubic GaN film. Nitrogen enrichment always led to a three-dimensional growth mode, while a coarse growth front led to an increase in the probability of forming GaN(0001) grains on (111) facets. But gallium enrichment leads to formation of gallium droplets, to a decrease in the growth rate, and hence to degradation of the film [97]. The best way to optimize the growth conditions is to control the structure of the growth front by RHEED in real time: when the RHEED patterns transform from spotted to striped, the film begins to grow in the layer-by-layer mode. High-quality cubic GaN films can be fabricated in just this way [97]. Another effective way to assist the growth of the β-GaN phase is to use surfactants, and the best of these is As [91]. For small fluxes, the local arrangement of the adsorbed As atoms proves to be the same as in bulk GaAs. Since GaAs crystallizes only into the zinc blende structure, the adsorption of As will hinder the formation of the wurtzite structure on the (111) facets but will facilitate the preferable growth of cubic GaN. Furthermore, the use of a substrate with a small lattice mismatch, e.g., cubic silicon carbide 3*C*-SiC(001), is also very useful for improving the quality of epitaxial β-GaN films.

6. Conclusions

By using the STM and RHEED methods under ultrahigh vacuum conditions, we were able to perform *in situ* studies of a number of ordered superstructures on the basal planes of the GaN surface. Hexagonal GaN films of both polarities were grown by plasma-assisted MBE methods on 6*H*-SiC(0001) and 6*H*-SiC(000$\bar{1}$) substrates, and films with cubic symmetry on GaAs(001)-2×4 substrates.

A new two-step method of cleaning the SiC surface has been developed. It includes high-temperature treatment of a sample in a hydrogen atmosphere and etching in an Si flux in an ultrahigh vacuum; depending on the substrate temperature and the intensity of the Si flux, a 3×3 or $\sqrt{3} \times \sqrt{3}$ reconstruction manifested itself on the 6*H*-SiC(0001) surface.

It was found that GaN films grown on the 6*H*-SiC(0001) substrate are Ga-polar, while those grown on the 6*H*-SiC(000$\bar{1}$) substrate are N-polar. The resulting polarity was determined by the preferential formation of N – Si and Ga – C/Al – C bonds at the interphase boundaries GaN/AlN/SiC. The two possible polarities of hexagonal GaN strongly affect the growth kinetics, chemical properties, and surface reconstructions, with the structure of the front of the growing surface playing the leading role in the fabrication of high-quality III-nitride films.

For the first time, a series of ordered 2×2, 4×4, 5×5, $5\sqrt{3} \times 2\sqrt{13}$, $\sqrt{7} \times \sqrt{7}$, and 10×10 structures and the pseudo 1×1-Ga fluid phase had been observed on the Ga-polar GaN(0001) surface. A comparison of the atomic-resolution STM images with the results of *ab initio* total energy calculations made it possible to develop a structural

model of the Ga adatom that describes the formation of the basic phases belonging to the $N \times N$ family. The quasi-one-dimensional structure proved to be characteristic of another group of surface reconstructions, to which the 5×2.5 and $5\sqrt{3} \times 2\sqrt{13}$ phases belong. This fact can be explained by the presence of Peierls distortions of the lattice of the adatoms located in the T_4 areas. All ordered phases are shown to be Ga-enriched and can be understood on the basis of the Ga-adatom scheme.

On the N-polar GaN(000$\bar{1}$) surface, a different family of structures was observed. This family includes the 2×3, 2×4, $\sqrt{7} \times \sqrt{7}$, $2\sqrt{7} \times 2\sqrt{7}$, 6×6, and 6×8 phases which are also Ga-enriched and can be understood on the basis of the Ga-adatom scheme. No stable phases induced by nitrogen have been observed on the two polar basal faces.

The exposure of the GaAs surface to a nitrogen plasma flux at the initial stages of growth of GaN films immediately led to the formation of a nitride layer with a 3×3 structure, which had a plain morphology and contained anisotropic vacancy islets. An increase in the time of exposure or in the substrate temperature was found to lead to a coarsening of the surface and to the formation of three-dimensional islets. The nitridation process was determined by the contribution of two competing mechanisms, namely, 3×3 ordering and continuous etching.

The formation of an atomically flat nitride layer with a 3×3 structure was found to play a crucial role in the formation of a GaN film with cubic symmetry, on which a 2×2 reconstruction was observed. But if the film growth took place on a coarse nitride surface, three-dimensional islands began to grow, and the film contained mixed cubic and hexagonal phases, while a $2\sqrt{7} \times 2\sqrt{7}$ reconstruction was observed on the surface. In this case, to grow high-quality GaN films of cubic symmetry it is advisable to use surfactants (such as As) or substrates with a small lattice mismatch.

Acknowledgments. The authors would like to thank Dr. T Ohno from the National Institute of Metals, Japan, for the help in doing *ab initio* calculations on a supercomputer.

This work has been supported by the Russian Foundation for Basic Research (grant 03-02-16402).

References

1. Nakamura S, Fasol G *The Blue Laser Diode: GaN Based Light Emitters and Lasers* (Berlin: Springer-Verlag, 1997)
2. Orton J W, Foxon C T *Rep. Prog. Phys.* **61** 1 (1998)
3. Ambacher O *J. Phys. D: Appl. Phys.* **31** 2653 (1998)
4. Pearton S J et al. *J. Appl. Phys.* **86** 1 (1999)
5. Szweda R *Gallium Nitride & Related Wide Bandgap Materials & Devices: a Market and Technology Overview 1998–2003* 2nd ed. (Oxford, UK: Elsevier Adv. Technol., 2000)
6. Jain S C, Willander M, Van Overstraeten R *Compound Semiconductors Strained Layers and Devices* (Boston: Kluwer Acad. Publ., 2000)
7. Kikkawa J M, Awschalom D D *Science* **287** 473 (2000)
8. Strite S, Morkoç H *J. Vac. Sci. Technol. B* **10** 1237 (1992)
9. Amano H et al. *Jpn. J. Appl. Phys. Pt. 2* **28** L2112 (1989)
10. Nakamura S et al. *Jpn. J. Appl. Phys. Pt. 1* **31** 1258 (1989)
11. Nakamura S, Mukai T, Senoh M *Appl. Phys. Lett.* **64** 1687 (1994)
12. Nakamura S *Science* **281** 956 (1998)
13. Popovici G, Morkoç H, Mohammad S N, in *Group III Nitride Semiconductor Compounds: Physics and Applications* (Ser. on Semiconductor Sci. and Technol., Vol. 6, Ed. B Gil) (Oxford: Clarendon Press, 1998) p. 16
14. Feenstra R M, Northrup J E, Neugebauer J *MRS Internet J. Nitride Semicond. Res.* **7** 3 (2002)
15. Hellman E S *MRS Internet J. Nitride Semicond. Res.* **3** 11 (1998)
16. Qian G-X, Martin R M, Chadi D J *Phys. Rev. B* **38** 7649 (1988)
17. Massalski T B (Editor-in-Chief) *Binary Alloy Phase Diagrams* Vol. 2, 2nd ed. (Materials Park, Ohio: ASM Intern., 1990) p. 1824
18. Held R et al. *J. Appl. Phys.* **85** 7697 (1999)
19. Masri P *Surf. Sci. Rep.* **48** 1 (2002)
20. Starke U *Phys. Status Solidi B* **202** 475 (1997)
21. Trampert A, Brandt O, Ploog K, in *Gallium Nitride* (GaN) *I* (Semiconductors and Semimetals, Vol. 57, Eds J I Pankove, T D Moustakas) (New York: Academic Press, 1998)
22. Okumura H et al. *J. Cryst. Growth* **178** 113 (1997)
23. Kurobe T et al. *Appl. Phys. Lett.* **73** 2305 (1998)
24. Lide D R (Ed.) *Handbook of Chemistry and Physics* (London: CRC Press, 1996) p. 76
25. Neumayer D A, Ekerdt J G *Chem. Mater.* **8** 9 (1996)
26. Pavlovska A, Bauer E, Smith D J *Surf. Sci.* **496** 160 (2002)
27. Bakhtizin R Z et al. *Usp. Fiz. Nauk* **167** 1227 (1997) [*Phys. Usp.* **40** 1175 (1997)]
28. Muehlhoff L et al. *J. Appl. Phys.* **60** 2842 (1986)
29. Kaplan R *Surf. Sci.* **215** 111 (1989)
30. Li L, Tsong I S T *Surf. Sci.* **351** 141 (1996)
31. Starke U et al. *Appl. Surf. Sci.* **89** 175 (1995)
32. Burk A A (Jr), Rowland L B *J. Cryst. Growth* **167** 586 (1996)
33. Owman F et al. *J. Cryst. Growth* **167** 391 (1996)
34. Xue Q et al. *Appl. Phys. Lett.* **74** 2468 (1999)
35. Bakhtizin R Z et al. *Poverkhnost'* (11) 4 (2000)
36. Martensson P, Owman F, Johansson L I *Phys. Status Solidi B* **202** 501 (1997)
37. Heine V, Cheng C, Needs R J *Am. Ceram. Soc. Bull.* **74** 2630 (1991)
38. Ohtani N et al. *Surf. Sci.* **398** L303 (1998)
39. Bernhardt J et al. *Appl. Phys. Lett.* **74** 1084 (1999)
40. Kimoto T, Itoh A, Matsunami H *Appl. Phys. Lett.* **66** 3645 (1995)
41. Bernhardt J et al. *Mater. Sci. Eng. B* **61–62** 207 (1999)
42. Starke U et al. *Surf. Rev. Lett.* **6** 1129 (1999)
43. Hoster H E, Kulakov M A, Bullemer B *Surf. Sci.* **382** L658 (1997)
44. Bermudez V M, Koleske D D, Wickenden A E *Appl. Surf. Sci.* **126** 69 (1998)
45. Ponce F A et al. *Appl. Phys. Lett.* **69** 337 (1996)
46. Smith A R et al. *Phys. Rev. Lett.* **79** 3934 (1997)
47. Smith A R et al. *Appl. Phys. Lett.* **72** 2114 (1998)
48. Smith A R et al. *J. Vac. Sci. Technol. B* **16** 1641 (1998)
49. Pashley M D *Phys. Rev. B* **40** 10481 (1989)
50. LaFemina J P *Surf. Sci. Rep.* **16** 137 (1992)
51. Rouviere J L et al. *Appl. Phys. Lett.* **73** 668 (1998)
52. Lin M E et al. *Appl. Phys. Lett.* **62** 702 (1993)
53. Hughes W C et al. *J. Vac. Sci. Technol. B* **13** 1571 (1995)
54. Hughes O H et al. *J. Vac. Sci. Technol. B* **16** 2237 (1998)
55. Iwata K et al. *Jpn. J. Appl. Phys.* **35** L289 (1996)
56. Foxon C T et al. *Surf. Sci.* **421** 377 (1999)
57. Thamm A et al. *Appl. Phys. Lett.* **75** 944 (1999)
58. Di Felice R, Northrup J E, Neugebauer J *Phys. Rev. B* **54** R17351 (1996)
59. Fritsch J et al. *Phys. Rev. B* **57** 15360 (1998)
60. Northrup J E, Di Felice R, Neugebauer J *Phys. Rev. B* **55** 13878 (1997)
61. Rapcewicz K, Nardelli M B, Bernholc J *Phys. Rev. B* **56** R12725 (1997)
62. Smith A R et al. *Appl. Phys. A* **66** S947 (1998)
63. Smith A R et al. *MRS Internet J. Nitride Semicond. Res.* **3** 12 (1998)
64. Smith A R et al. *Surf. Sci.* **423** 70 (1999)
65. Xue Q-K et al. *Phys. Rev. Lett.* **82** 3074 (1999)
66. Stroscio J A, Kaiser W J (Eds) *Scanning Tunneling Microscopy* (Boston: Academic Press, 1993)
67. Bakhtizin R Z et al. *Poverkhnost'* (11) 9 (2000)
68. Vanderbilt D *Phys. Rev. B* **41** 7892 (1990)
69. Ramachandran V et al. *J. Cryst. Growth* **209** 355 (2000)
70. Ramachandran V et al. *Appl. Phys. Lett.* **75** 808 (1999)
71. Vézian S et al. *Surf. Sci.* **541** 242 (2003)
72. Peierls R E *Quantum Theory of Solids* (Oxford: Clarendon Press, 1955) p. 108
73. Neugebauer J et al. *Phys. Rev. Lett.* **80** 3097 (1998)

74. Grüner G *Density Waves in Solids* (Reading, Mass.: Addison-Wesley, 1994); Grüner G, Zettl A *Phys. Rep.* **119** 117 (1985)
75. Duke C B *Appl. Surf. Sci.* **65/66** 543 (1993)
76. Xue Q-Zh et al. *Phys. Rev. B* **59** 12604 (1999)
77. Bakhtizin R Z et al. *Phys. Low-Dim. Struct.* (3/4) 243 (2001)
78. Smith A R et al. *J. Vac. Sci. Technol. B* **16** 2242 (1998)
79. Northrup J E et al. *Phys. Rev. B* **61** 9932 (2000)
80. Xie M H et al. *Phys. Rev. Lett.* **82** 2749 (1999)
81. Capaz R B, Lim H, Joannopoulos J D *Phys. Rev. B* **51** 17755 (1995)
82. Ponce F A, Van de Walle C G, Northrup J E *Phys. Rev. B* **53** 7473 (1996)
83. Visconti P et al. *Phys. Status Solidi B* **228** 513 (2001)
84. Zyweitz T, Neugebauer J, Scheffler M *Appl. Phys. Lett.* **73** 487 (1998)
85. Feuillet G et al. *Appl. Phys. Lett.* **70** 1025 (1997)
86. Tarsa E J et al. *J. Appl. Phys.* **82** 5472 (1997)
87. Bakhtizin R Z et al. *Zh. Eksp. Teor. Fiz.* **111** 1858 (1997) [*JETP* **84** 1016 (1997)]
88. Daudin B et al. *J. Appl. Phys.* **84** 2295 (1998)
89. Schikora D et al. *Phys. Rev. B* **54** R8381 (1996)
90. Brandt O et al. *Phys. Rev. B* **52** R2253 (1995)
91. Okumura H et al. *Appl. Phys. Lett.* **72** 3056 (1998)
92. Heller E J, Zhang Z Y, Lagally M G *Phys. Rev. Lett.* **71** 743 (1993)
93. Trampert A et al. *Appl. Phys. Lett.* **70** 583 (1997)
94. Gwo S, Tokumoto H, Miwa S *Appl. Phys. Lett.* **71** 362 (1997)
95. Bykhovski A D, Shur M S *Appl. Phys. Lett.* **69** 2397 (1996)
96. Yang H et al. *Appl. Surf. Sci.* **104/105** 461 (1996)
97. Ploog K H et al. *J. Vac. Sci. Technol. B* **16** 2229 (1998)
98. Yeh C-Y et al. *Phys. Rev. B* **46** 10086 (1992)